Photocatalytic activity of CuO nanoparticles for organic and inorganic pollutants removal in wastewater remediation

Assefu Kassegn Sibhatu [a], Getu Kassegn Weldegebrieal [b*], Suresh Sagadevan [c*], Nam Nghiep Tran[d] and Volker Hessel[d*]

[a]Department of Physics, College of Natural and Computational Sciences, Debre Berhan University, Ethiopia

[b]Department Chemistry, College of Natural and Computational Sciences, Debre Berhan University, Ethiopia

[c]Nanotechnology & Catalysis Research Centre, University of Malaya, Kuala Lumpur 50603, Malaysia

[d]School of Chemical Engineering and Advanced Materials, The University of Adelaide, North Terrace Campus, Adelaide 5005, Australia

[*]Corresponding author e-mail: belay.kassegn@gmail.com; drsureshnano@gmail.com; volker.hessel@adelaide.edu.au

Abstract

Heterogeneous photocatalysis is a promising technology for eradicating organic, inorganic, and microbial pollutants in water and wastewater remediation. It is a more preferable method to other conventional wastewater treatment approaches on account of its low cost, environmental benignity, ability to proceed at ambient temperature and pressure conditions, and capability to completely degrade pollutants under appropriate conditions into environmentally safe products. In heterogeneous photocatalysis, pollutant removal is mainly induced by in-situ generated reactive radicals and their subsequent attack when energetic radiation impinges on the semiconductor catalyst. As such, for the effective and economical removal of wastewater pollutants, the employed catalyst should have high photonic efficiency, less toxic, abundant, chemically and photochemically stable, visible light active, and easily synthesized. Copper (II) oxide (CuO) is one

such substance acting as a catalyst that has been hampered primarily by rapid recombination and slow mobility of photogenerated charge carriers. So, this review provides an overview of the strategies adopted to mitigate the aforementioned drawbacks and also other operational parameters to boost its catalytic activity towards the elimination of toxic organic and inorganic metal ion contaminants in an aqueous media. As such, we believe that it will serve as valuable input in the design and development of competent transition metal oxide-based photocatalysts in practical wastewater remediation.

Keywords: Cupric oxide, Heterogeneous photocatalysis, Organic pollutants, Toxic heavy metal ions, Wastewater remediation

1. Introduction

Clean and safe water is a vital commodity for humans' survival. It is used in multiple applications including for drinking, food preparation, business, and irrigation purpose. Though about 71% of the surface of the Earth is covered with water, only nearly 3% of it is freshly available locked up in the form of glaciers and ice and of which a very minute fraction, available in liquid form on the surface in rivers, lakes and the atmosphere (Khatri and Tyagi, 2015). Natural and primarily anthropogenic activities are the causes of water contamination. On account of its, extremely varied composition including organic, inorganic, and biological contaminants, wastewater can be a threat to the environment and humans' health unless properly managed (Kodavanti et al., 2014; Srivastav and Ranjan, 2020). Thus, wastewater treatment is a crucial step to avoid not only its potential consequences but also the shortage of clean and safe water and ensure its sustainable utilization.

Wastewater treatment methods can generally be classified as physical, chemical, biological, or a hybrid of these. While in the physical method, physical pollutants of wastewater such as suspended solid particles and floating oil or foam are removed by settling and skimming from the top surface, respectively, the chemical method involves the deliberate addition of chemicals to act as flocculants to promote precipitation of dissolved substances or as disinfecting agents such as chlorine, ozone or chlorine dioxide to neutralize microorganisms. In the biological treatment method, microorganisms are utilized to break down organic pollutants from wastewater through normal cellular processes. Conventional wastewater treatment approaches including adsorption on activated carbons, chemical oxidation and reduction, chemical precipitation, flocculation, flotation, and so on (Weldegebrieal, 2020b; Shrestha et al., 2021) are costly and do not involve the destruction of pollutant substances (Muhd Julkapli et al., 2014). However, due to the complex nature of the wastewater matrix, adequate decontamination of wastewater is difficult to achieve and in practice, a combination of the mentioned methods is employed to get quality water more economically (Crini and Lichtfouse, 2019).

Advanced oxidation processes (AOPs) are wastewater treatment methods in which the pollutants are removed by redox reactions of in situ generated hydroxyl radicals. Such systems include the addition of ozone (O_3), UV/O_3, UV/H_2O_2, UV/O_3/H_2O_2, Fe^{2+}/H_2O_2 (Fenton's reagent), etc. The advantages of these systems include fast reaction kinetics, small footprint in the treated water, no formation of sludge and hence reduced cost of treatment, can proceed at mild temperature and pressure conditions, can completely degrade pollutants under appropriate conditions, are simpler to operate, and are easily integrable with other treatment approaches (Rajamanickam and Shanthi, 2016; Garrido-Cardenas et al., 2020). Nevertheless, the high cost of chemical utilization needed to maintain the operation of the system is one of their main shortcomings.

Heterogeneous photocatalysis is one of the AOPs which can be defined as radiation–assisted acceleration of the rate of chemical reactions in the presence of semiconductor photocatalyst. Here, reactive radical species such as hydroxyl radical ($HO^{\cdot}$) and superoxide radical ion ($O_2^{-\cdot}$) are formed when photons of incident radiation promote electrons from the valence band (VB) to the conduction band (CB) of the semiconductor, leaving holes behind in the VB and then the VB holes and CB electrons oxidize and reduce water and dissolved oxygen gas, respectively. Once generated, these reactive radicals decompose the pollutants into less harmful products (Joseph et al., 2009; Sonu et al., 2019; Sharma et al., 2021). As compared to conventional wastewater treatment techniques, heterogeneous photocatalysis is a preferable option owing to its advantages such as ease of application, less costly as only a small amount of catalyst and sunlight may be used to run the degradation reactions, which can proceed at ambient conditions, environmentally friendly, and involves the elimination of pollutants rather than transferring them from one phase to another as in the case of adsorption (Sharma et al., 2019; Sonu et al., 2019; Hasija et al., 2021a). The heart of heterogeneous photocatalytic reactions is the photocatalyst, different types of photocatalysts such as cadmium sulfide (CdS)-based (Sharma et al., 2021), cobalt ferrite ($CoFe_2O_4$) (Sonu et al., 2019), bismuth oxyhalides (BiOX, X = F, Cl, Br, I) (Sharma et al., 2019; Yao et al., 2021), ZnS or MoS_2/ZnS embedded in N/S doped carbon (Al-Kahtani et al., 2019; Ahamad et al., 2020a), multivariate metal organic frame works (MOF) (Patial et al., 2021), zeolithic imidazolate framework 8 (ZIF-8)/graphitic carbon nitride (g-C_3N_4), that is ZIF-8/g-C_3N_4 (Qiu et al., 2021b), MOF-derived carbons (Hao et al., 2021), covalent organic frameworks-based single metal atom catalysts (Hasija et al., 2022), MXenes (family of 2D transition metal nitrides and/or carbides), biochar-based materials (Yu et al., 2022), g-C_3N_4-based (Hasija et al., 2021b; Kumar et al., 2021; Liu et al., 2021), etc have been developed and excellently reviewed recently

for the elimination of diverse organic and inorganic pollutants in wastewater. Transition metal oxides are interesting photocatalysts because of their easier synthesis and ability to form different metal-oxygen ratios, due to their half-filled d orbitals that enable them to form different oxidation states, with varying properties and catalytic pollutants removal performance (Cui et al., 2015; Pareek and Venkata Mohan, 2019; Zhang et al., 2021).

Copper (II) oxide or cupric oxide (CuO) is a transition metal oxide having numerous applications in different fields. It is an intrinsically p-type semiconductor owing to oxygen vacancy defects in its crystal structure and has an indirect narrow bulk bandgap of 1.2 eV at RT (Dhineshbabu et al., 2016). It has monoclinic crystal structure with space group C2/c and lattice constants of a = 4.6837, b = 3.4226, c = 5.1288 Å, and β = 99.54° (Tiginyanu et al., 2011). Copper (I) oxide or cuprous oxide (Cu_2O) and copper (III) oxide (Cu_4O_3) are other polymorphs and while Cu_2O is a thermally less stable phase than CuO, Cu_4O_3 is a metastable phase with a mixed oxidation state of Cu atom and is difficult to synthesize (Wang et al., 2016; Murali and Aryasomayajula, 2018). CuO nanostructures with various physicochemical properties have generally been synthesized using physical methods such as mechanical ball-milling and laser ablation, a chemical method such as sol-gel, microemulsion, solvothermal, etc., and biological methods using plant extracts (Weldegebrieal, 2020a). These have been used in diverse applications including in magnetic storage media, high-temperature superconductors, as an electrode in dye-sensitized solar cells, lithium-ion batteries, and solid oxide fuel cells, in chemical and gas sensors, catalysis, pharmacy in antitumor therapy, as an antimicrobial agent in food preservation, biomedicine to prevent bacterial infection of biomedical devices, textile to produce antibacterial textile fabrics, and in photocatalysis to decompose organic pollutants from water or wastewater (Tadjarodi et al., 2015; Aminuzzaman et al., 2017; Vaidehi et al., 2018; Verma and Kumar, 2019; Akintelu et al., 2020;

Weldegebrieal, 2020b; Phang et al., 2021). Such features as low cost and easy availability of starting materials, excellent chemical and photochemical stability, visible light activity owing to its narrow band gap, and facile synthesis make CuO nanostructures interesting to researchers in the photocatalytic eradication of pollutants from wastewater (Ighalo et al., 2021). However, fast charge carrier recombination and a low specific surface area along with utilized operational parameters are prominent drawbacks that hinder its efficiency and widespread application in photocatalysis. Although heterogeneous photocatalytic reactions are generally difficult to understand completely due to the complex nature of the reaction, studying the influence of the physicochemical properties of the catalyst as well as the influence of experimental parameters, that are often overlooked in many reports, is crucial to ensure efficient utilization of catalysts in the removal of pollutants in wastewater. In this regard, the main objectives of this review are: (1) to overview the photocatalytic activity response of CuO NPs synthesized using different synthesis protocols towards the destruction of various organic and inorganic pollutants; (2) to discuss the influence of operational parameters on the degradation performance; (3) to study the mechanism of organic and inorganic pollutants removal using CuO and CuO-based photocatalysts; (4) to provide the current challenges that still need to overcome in producing highly efficient CuO and CuO-based photocatalysts, from authors' perspectives, so that they may be used for large-scale application for the treatment of wastewater based on latest reports in the literature. To the best of the authors' knowledge, no such work has been reported before.

2. Photocatalytic activity of CuO nanoparticles

Wastewater may bear physical, chemical and biological impurities of which organic and inorganic pollutants discharged from various sources are very common. CuO nanostructures are one among many interesting photocatalysts utilized by researchers for the eradication of these

pollutants under their abundance, low cost, narrower bandgap, excellent chemical and photochemical stability, and facile synthesis (Sapkota et al., 2020). Comparatively, there is a large volume of literature reports of photocatalytic activity of CuO and CuO-based photocatalysts to organic pollutants degradation than for inorganic metal ions removal, which we will discuss separately in the following sections.

2.1 Photocatalytic activity of CuO NPs for organic pollutants

Being a semiconductor with a narrow bandgap, CuO is active in the visible wavelength region of the electromagnetic spectrum. The conspicuous advantage of this is that sunlight whose predominant radiation reaching the surface of the earth is visible which may be used to stimulate the photocatalytic decomposition process of organic pollutants; however, the drawback associated with it is the high probability of photogenerated e^-/h^+ pairs recombination which suppresses the photonic and hence removal efficiency. As a consequence, improving some of its surface morphological properties via improved synthetic route and optimizing experimental parameters are crucial to maximize the degree of decomposition of organic contaminants in water and wastewater reclamation using CuO NPs as photocatalysts. Before directly delving the photocatalytic activity of CuO and CuO-based catalysts to organic pollutants for the rate of photodegradation reaction, reactive species responsible for decomposition, and catalyst recoverability and reusability, which is an important factor for its industrial large-scale application.

2.1.1 Mechanism of photocatalytic decomposition of organic pollutants

Photocatalytic decomposition of organic pollutants using semiconductor photocatalysts may occur through direct or indirect mechanistic routes. In the direct mechanism, the hydroxyl radical ($HO^{\cdot}$) and superoxide radical ion ($O_2^{-\cdot}$), the two reactive radicals mainly responsible for the

degradation of pollutants, are generated in the reaction system by the direct injection of photoexcited electrons from the pollutant organic molecules (OM^*) into the CB of the semiconductor, where it gets itself oxidized to give radical cation ($OM^{+\cdot}$) and reduces dissolved O_2 to $O_2^{-\cdot}$, Eq. (8-9) and then to $HO^\cdot$ via a sequence of steps as shown in Eq. (5-7) and graphically illustrated in Figure 1(1).

$$CuO + h\nu \rightarrow CuO\,(e^- + h^+) \quad (1)$$

$$O_2 + e^- \rightarrow O_2^{-\cdot} \quad (2)$$

$$H_2O + h^+ \rightarrow HO^\cdot + H^+ \quad (3)$$

$$HO^- + h^+ \rightarrow HO^\cdot \quad (4)$$

$$O_2^{-\cdot} + H^+ \rightarrow HOO^\cdot \quad (5)$$

$$2HOO^\cdot \rightarrow H_2O_2 + O_2 \quad (6)$$

$$H_2O_2 \rightarrow 2HO^\cdot \quad (7)$$

$$OM + h\nu \rightarrow OM^* \quad (8)$$

$$OM^* + O_2 \rightarrow O_2^{-\cdot} + OM^{+\cdot} \quad (9)$$

$$OM + OM^{+\cdot} + HO^\cdot/O_2^{-\cdot} \rightarrow \text{Decomposed products} \quad (10)$$

However, in the indirect route, Figure 1(2), the first electron-hole (e^-/h^+) pairs are formed when electromagnetic radiation of energy ($h\nu$) greater than or equal to the bandgap energy (E_g) of the semiconductor catalyst (CuO) irradiates it and excites electrons from the valence band (VB) to the conduction band (CB), leaving holes behind in the VB. Then, these e^-/h^+ pairs may recombine giving off the excess energy in the form of heat or radiation or undergo separate redox reactions by diffusing onto the surface and reacting with nearby surface adsorbed species. That is, the photoexcited electrons reduce adsorbed O_2 to $O_2^{-\cdot}$ While the holes oxidize H_2O or HO^- to $HO^\cdot$, Eq. (1-4). So, any strategy that minimizes the recombination and maximizes the separation of the photoproduced charge carriers results in an augmented rate of degradation.

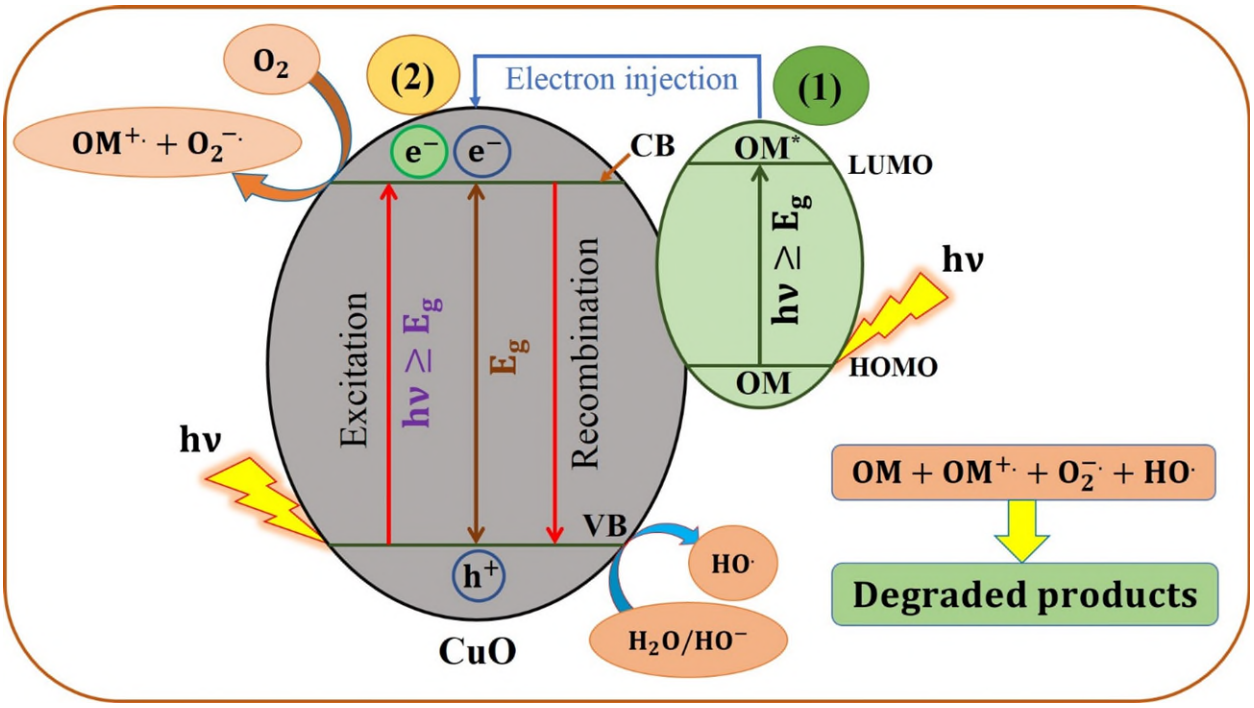

185

186 **Figure 1.** Photocatalytic degradation mechanism of organic molecule (OM) pollutant using CuO
187 photocatalyst (Sibhatu et al., 2022).

188 It has been found that the indirect mechanism is kinetically faster and the predominant route
189 in the photocatalytic degradation of organic pollutants (Ajmal et al., 2014). The oxidation reactions
190 of VB holes and reduction reactions of CB electrons with catalyst surfaces adsorbed species are
191 essential in achieving the separation of photogenerated charge carriers and promoting the rate of
192 pollutants removal. The electron transfer mechanism and efficiency of charge carriers' separation
193 could be different from catalyst to catalyst depending on the size of the bandgap and whether the
194 catalyst is single phase, doped or is a mixed phase. After they are in situ produced, the reactive
195 radicals start off attacking the pollutant compounds via hydrogen abstraction, electron transfer,
196 radical addition and combination modes (Pirilä et al., 2015). Even though the exact mechanistic
197 route leading to the eventual mineralization of organic pollutants is difficult to track due to the
198 complex nature of the reaction, rough routes by which the destruction occurs could be proposed

based on experimental evidence from, for example, GC-MS or LC-MS results of reaction mixture taken at the initial, intermediate, and final stages of the photodegradation reaction.

As a consequence, researchers have proposed various possible photocatalytic decomposition mechanistic pathways for different organic pollutants in water and wastewater. For instance, Bhattacharjee and Ahmaruzzaman (Bhattacharjee and Ahmaruzzaman, 2016) reported that during the photocatalytic degradation of methylene blue identification of the fragmentation products from the mass spectra from LC-MS data showed the breakage of the dye molecules along the broken line denoted by "b" (Figure 2) in the thiazine ring to produce intermediate phenol and p-aminophenol products before undergoing further oxidation to give CO_2, H_2O and mineral acids. Whereas, fragmentation of the same molecules during photocatalytic degradation reactions using Cu_2O photocatalysts was proposed to be along the broken line denoted by "a" based on evidence obtained from LC-MS data (Mrunal et al., 2019). In another study, Rao *et al.* (Rao et al., 2017) proposed the degradation mechanism of tartrazine dye in the presence of CuO straw-sheaf-like nanostructures utilizing evidence obtained from GC-MS result of a sample taken at an intermediate stage of the photodegradation reaction, Figure 3.

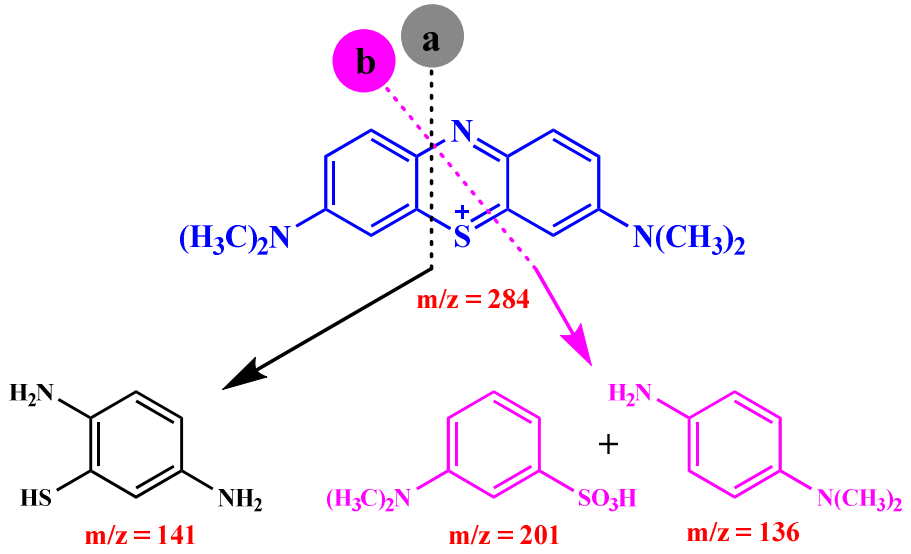

214

215 **Figure 2.** Fragmentation pathway of MB during photocatalytic degradation along the broken lines
216 denoted by (a) and (b) to give the indicated intermediate products (Bhattacharjee and Ahmaruzzaman,
217 2016; Mrunal et al., 2019).

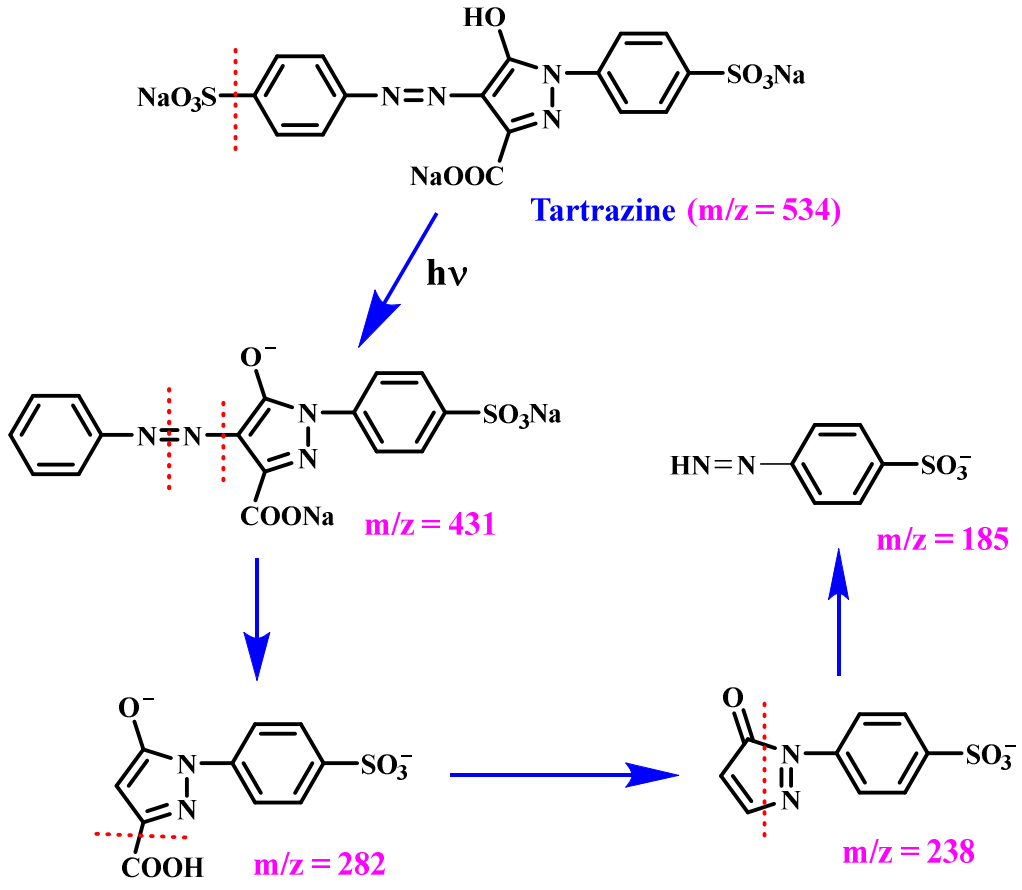

218

219 **Figure 3.** Proposed degradation pathway of tartrazine dye using CuO nanostructures (Rao et al., 2017).

Here, the C-S bond of the parent tartrazine molecule of m/z = 534 is cleaved to produce a daughter molecule of m/z = 431. This molecule, in turn, undergoes further cleavage of bonds, along the indicated broken lines, to produce the indicated intermediate molecules.

Additionally, Raha *et al.* (Raha et al., 2021) proposed the likely degradation pathway during the pharmaceutical drug rabeprazole photodegradation reaction using $CuO/Mn_3O_4/ZnO$ nanocomposite catalyst by utilizing the HRLC-MS result performed in the intermediate stage of the reaction, to involve three steps, Figure 4. In step I, the parent rabeprazole molecule undergoes C-S bond cleavage to produce two daughter molecules of mass 118 and 243. In step II, the molecule with mass 243 is fragmented into two molecules of mass 171 and 74 upon cleavage of the C-O bond. In step III, the molecule with mass 171 is further decomposed into smaller intermediate molecules of mass 105 and 72, which are further decomposed into smaller molecules in the subsequent steps. Karthikeyan *et al.* (Karthikeyan et al., 2019), using information from HPLC analysis, proposed the Cu_2O/CuO catalyst-assisted photodecomposition mechanism of N-acetyl-para-aminophenol. Their outline involves first the formation of hydroquinone from the parent molecule via $HO^{\cdot}$ attack to give benzoquinone and then fumaric acid, maleic acid, and oxalic acid molecules in the latter ring-opening step, Figure 5. In another study of the photocatalytic degradation of Allura red dye utilizing porous CuO nanosheets as photocatalysts under UV-vis light illumination in the presence of $NaBH_4$ as a reducing agent, the decomposition mechanism was proposed to proceed first through the breakage of the most susceptible azo (-N=N-) linkage in the dye to produce the colorless amine derivatives, Figure 6, and then into CO_2 and H_2O at the end of the decomposition process (Nazim et al., 2021).

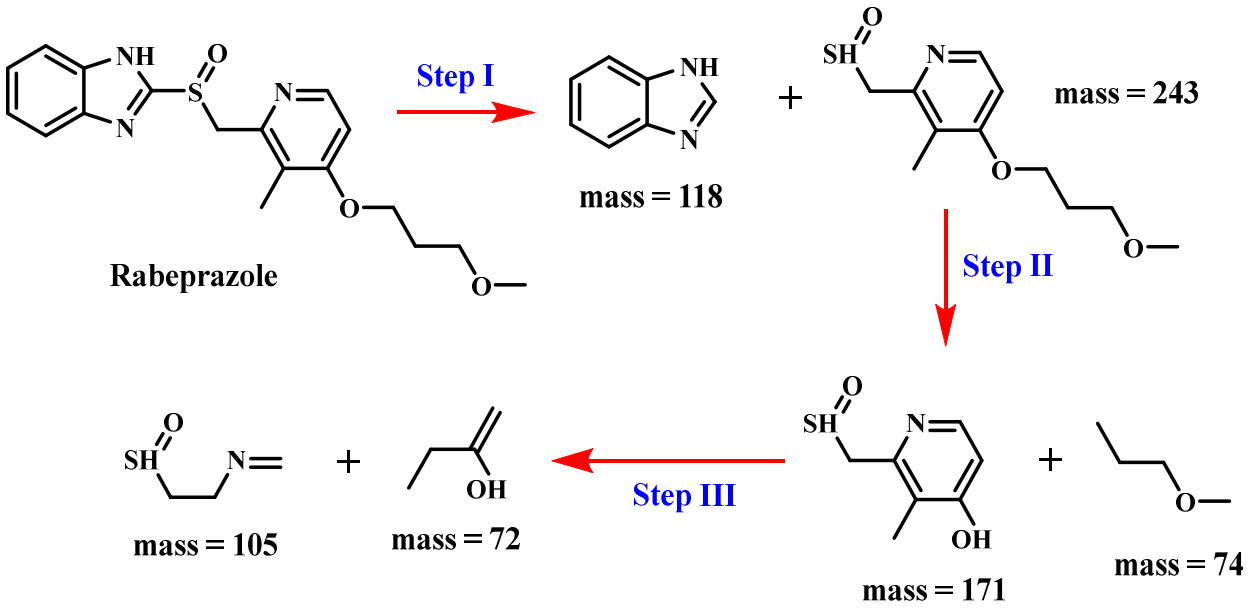

Figure 4. Proposed photocatalytic degradation mechanism of rabeprazole molecules using $CuO/Mn_3O_4/ZnO$ nanocomposite (Raha et al., 2021).

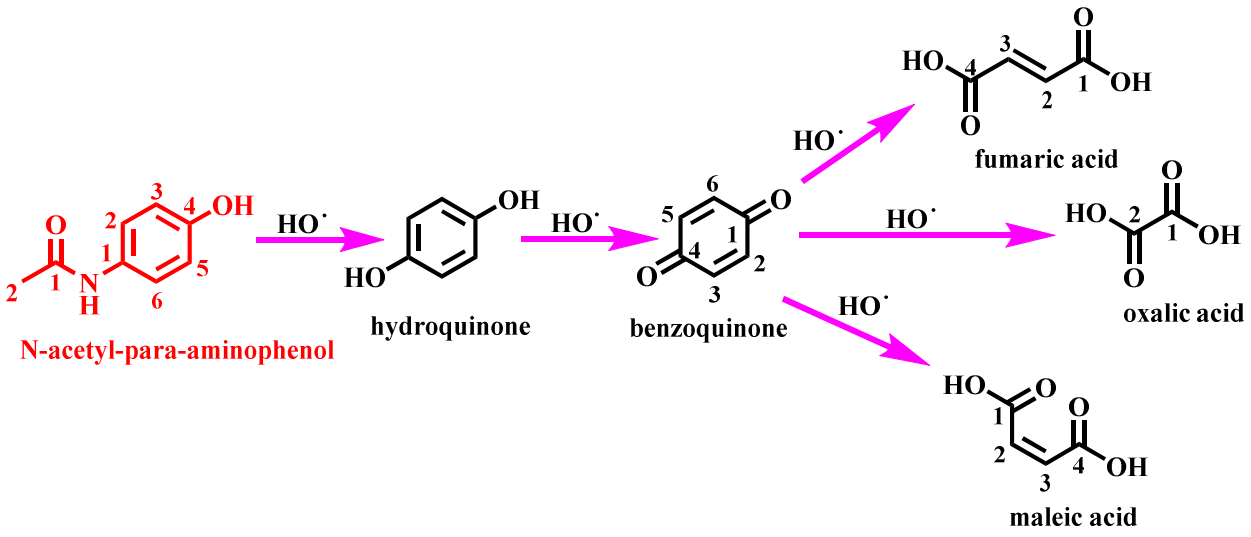

Figure 5. Proposed photocatalytic degradation pathway for N-acetyl-para-aminophenol using core-shell $Cu_2O@CuO$ catalyst (Karthikeyan et al., 2019).

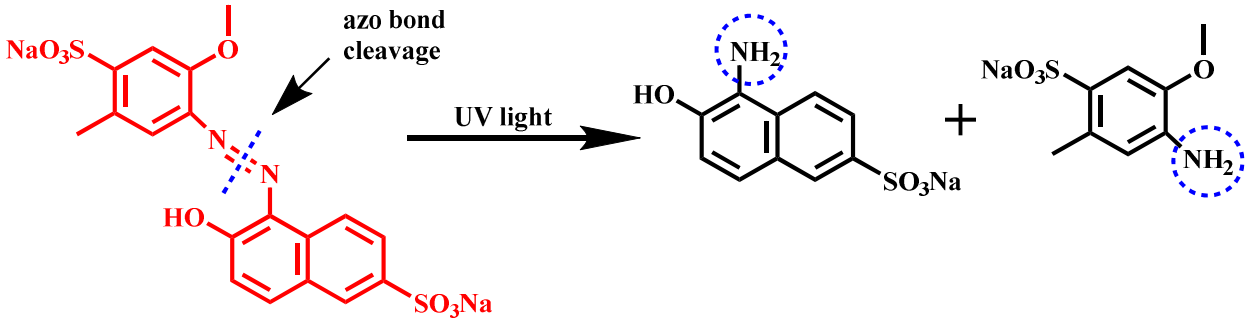

Figure 6. Degradation products of Allura red dye using CuO catalyst. Adapted from reference (Nazim et al., 2021).

From the degradation mechanisms discussed above, one can see that it is difficult to predict the exact degradation pathway unless there is a live method of attending to the progress of the reaction up to a certain stage. Nonetheless, determining the composition of the reaction in different stages of the reaction is indispensable to ensure the degree of completion of the reaction as visual color change alone may not be enough to indicate the degree of mineralization since it is possible to end with colorless intermediate products that are often harmful end products as compared to the starting pollutants.

2.1.2 Test for reactive species

Although the whole process for the photocatalytic degradation of organic pollutants is still unclear, the contributions made by reactive species can be determined using evidence from electron paramagnetic resonance (EPR) spectroscopy and scavenging test (Qiu et al., 2021a). In the scavenging test, the degradation reactions are carried out in the presence of scavengers for reactive species such as holes (h^+), electrons (e^-), superoxide radical ion ($O_2^{-\cdot}$), and hydroxyl radical ($HO^{\cdot}$) and information about their likely participation in the degradation process is acquired. The percentage of degradation will be retarded in the presence of scavenging species if the species

have played their role in the process of decomposition reaction. For quenching $HO^{\cdot}$ radical, usually, isopropanol or t-butanol is added, and benzoquinone or ascorbic acid are employed to test for $O_2^{-\cdot}$ (Neena et al., 2018; Weldegebrieal et al., 2021). In addition, while salts such as $NaSO_4$ or $NaNO_3$ are used for testing hydrated e^-, KI, EDTA, ammonium oxalate, etc are used for testing photogenerated h^+ (Weldegebrieal and Sibhatu, 2021). So, using information obtained from the scavenging tests, the main reactive species that participated in the degradation process may be proposed. Chauhan *et al.* (Chauhan et al., 2020) investigated the likely involvement of $HO^{\cdot}$ during the degradation of Victoria blue and direct red 81 dyes taken separately in the presence of CuO NPs and the scavengers of DMSO and carbonate ion. They found that the decomposition decreased in the presence of the scavengers, confirming the participation of the radicals in the degradation process. In another study reported by Haseena *et al.* (Haseena et al., 2019), test or reactive $HO^{\cdot}$, h^+, and $O_2^{-\cdot}$ Species using the respective scavengers of isopropyl alcohol, triethanolamine, and p-benzoquinone, have found that removal efficiency of rhodamine B using biosynthesized CuO NPs photocatalysts decreased by 44 and 32% in the presence of the first two respective trappers meanwhile no significant reduction was seen in the presence of $O_2^{-\cdot}$ scavenger, indicating that $HO^{\cdot}$ and h^+ are primarily engaged in the degradation process of the dye. Whereas, inhibition of the photocatalytic decomposition of methylene blue using CuO-Cu_2O catalyst in the presence of t-butanol, ammonium oxalate, and benzoquinone added as scavengers for $HO^{\cdot}$, H^+, and $O_2^{-\cdot}$ indicated that all three reactive radicals have possibly participated in the degradation reaction of the dye though the inhibition was greatest in the presence of $HO^{\cdot}$ radical (Dasineh Khiavi et al., 2019). Further details of the types of reactive species that induced the photocatalytic degradation of organic pollutants using CuO-based photocatalysts have been recently reviewed in reference (Raizada et al., 2020).

2.1.3 Catalyst recoverability and reusability

One of the merits of heterogeneous photocatalysis that makes it cost-effective is that a small amount of catalyst is required and it may be used repeatedly. Nonetheless, catalyst spending due to chemical or photochemical corrosion and colloid formation is often a challenge with some catalysts used in slurry form. Generally, CuO is a photochemically stable catalyst but the slight particle agglomeration that occurs during recycling could hinder its photocatalytic performance retention (Chauhan et al., 2020). The recoverability of a catalyst or adsorbent is an important factor for their commercial application. While the separation of magnetic materials such as magnetite (Fe_3O_4) and its derivatives from solution can be easily facilitated with the aid of external magnets (Ahamad et al., 2020b), for non-magnetic materials such as CuO used in slurry form, it becomes costly and time-consuming process (Ahamad et al., 2019). One strategy to minimize such problems can be to use the catalyst in a fixed-bed form on suitable substrates though this alternative has also its shortcomings (Umar and Aziz, 2013). Several recyclability tests of CuO-based materials for the photodegradation of organic pollutants have been conducted. For example, Pakzad *et al.* (Pakzad et al., 2020) found a slight change in the removal efficiency of the antibiotic cephalexin utilizing magnetic Fe_3O_4@CuO nanoparticles as a catalyst after 5 cycles with only about 10% reduction in efficiency after the 7^{th} cycle. In a report by Munawar *et al.* (Munawar et al., 2021), a test of the MgO-ZnO-CuO ternary composite photocatalyst stability by successive collection of particles by centrifugation, washing and drying exhibited efficiency fading by less than 4%, from 98.8% degradation to 95% degradation, after the 5^{th} cycle to the photodegradation of P-nitroaniline.

In general, as catalyst recoverability and reusability are essential factors in its large-scale application, synthesis methods need to consider ways of maximizing these factors while ensuring efficient photodegradation of target pollutants.

2.1.4 Kinetics of photocatalytic degradation reactions of organic pollutants

For photocatalytic degradation reactions, the photocatalyst, organic pollutant, and radiation should be in contact or proximity for the reactions to proceed and the pollutant's concentration goes decrease with time if the employed catalyst is photoactive to the contaminant molecules under the given experimental condition. The extent of elimination or degradation (D%) of the pollutant can be obtained by observing the change in its absorbance or concentration with time using Eq. (11),

$$\mathrm{D}\ (\%) = \left(\frac{\mathrm{A_0} - \mathrm{A_t}}{\mathrm{A_0}}\right) \times 100 = \left(\frac{\mathrm{C_0} - \mathrm{C_t}}{\mathrm{C_0}}\right) \times 100 \qquad (11)$$

Where $\mathrm{A_0}$, $\mathrm{C_0}$, $\mathrm{A_t}$, and $\mathrm{C_t}$ are the absorbance and concentration values initially before radiation exposure and after exposure time (t), respectively.

Regarding the kinetics of the reaction, the heterogeneous photocatalytic degradation reactions of organic pollutants mainly obey pseudo-first-order kinetics. That is the time rate of change of the concentration of the pollutant is first-order in the concentration of the pollutant and is given by Eq. (12),

$$-\frac{\mathrm{dC}}{\mathrm{dt}} = \kappa_1 \mathrm{C} \qquad (12)$$

Where, C is pollutant concentration and κ_1 is the pseudo-first-order reaction rate constant.

Rearranging and integrating Eq. (12) without limits gives,

$$-\int \left(\frac{\mathrm{dC}}{\mathrm{C}}\right) = \kappa_1 \int \mathrm{dt} \ \Rightarrow \ln \mathrm{C} = \ -\kappa_1 \mathrm{t} \qquad (13)$$

Integrating Eq. (12) with limits at $\mathrm{t} = 0, \mathrm{C} = \mathrm{C_0}$ and at $\mathrm{t} = \mathrm{t}, \mathrm{C} = \mathrm{C_t}$ gives,

$$\ln\left(\frac{\mathrm{C_t}}{\mathrm{C_0}}\right) = -\kappa_1 \mathrm{t} \Rightarrow \ln\left(\frac{\mathrm{C_0}}{\mathrm{C_t}}\right) = \kappa_1 \mathrm{t} \qquad (14)$$

Then, if the plot of $\ln\left(\frac{C_0}{C_t}\right)$ versus t of the experimental data give a good fit, coefficient of correlation (R^2) close enough to 1, with the generated linear regression line, then the reaction could be satisfactorily described using pseudo-first-order kinetics model. One measure of the goodness of fit between the model and experimental data is the coefficient of correlation (R^2) and a value greater than or equal to 80% is suggested to be good for model validation (Revellame et al., 2020). In some cases, pseudo-second-order kinetics are also reported to have better fitted experimental data to the model linear regression line. In pseudo-second-order kinetics, the rate of the reaction is second order in pollutant concentration, Eq. (15),

$$-\frac{dC}{dt} = -\kappa_2 C^2 \tag{15}$$

Rearranging and integrating without limits of Eq. (15) gives Eq. (16),

$$-\int \left(\frac{dC}{C^2}\right) = \kappa_2 \ dt \Rightarrow -\frac{1}{C} = \kappa_2 t \tag{16}$$

But integration in the limits at $t = 0, C = C_0$ and $t = t, C = C$, gives

$$\frac{1}{C} = -\kappa_2 t + \frac{1}{C_0} \tag{17}$$

Where, C_0 and C_t are the initial and final concentrations of the pollutant.

From first-order kinetics, the best fit of the experimental data to the linear regression line up on plotting $\frac{1}{C}$ versus t indicates that the reaction kinetics could be described using the pseudo-second-order model.

The relative kinetics of photocatalytic reactions can be compared with the half-life period in a similar duration of degradation reactions. The half-life of a reaction is the time it takes to reduce the initial concentration of the pollutant by half and is independent of the initial concentration of the dye used for first-order reactions, Eq. (18),

$$t_{1/2} = \frac{\ln(2)}{\kappa_1} \quad (18)$$

Where, κ_1 is the first-order reaction rate constant. The shorter the half-life, the faster the reaction and vice versa.

Unlike a pseudo-first-order reaction, the half-life of 2nd order reaction depends on the initial concentration and is given by Eq. (19),

$$t_{1/2} = -\frac{1}{C_0 \kappa_2} \quad (19)$$

Where, C_0 and κ_2 refer to the initial concentration of the organic pollutant and the second-order reaction rate constant, respectively.

The rate of photodegradation reaction is also an important factor that needs to be considered during degradation reactions and a catalyst with a high reaction rate constant will be the first choice provided other factors are kept constant.

2.1.5 Factors affecting photocatalytic degradation of organic pollutants

Photocatalytic degradation reactions are complex processes in which the elimination efficiency of organic pollutants depends on several factors. Much as other semiconductor photocatalysts, the extent of photocatalytic decomposition of the pollutants depends on such factors as morphological properties of the synthesized CuO and CuO-based catalysts, type of organic pollutant, operational parameters such as catalyst dose and pollutant initial concentration, pH, temperature, aeration and stirring rate, energy and intensity of employed radiation, and the presence of oxidants and other interferents in the reaction mixture, which are reviewed individually as under.

2.1.5.1 Effect of morphological properties of CuO and CuO-based catalysts on the degradation efficiency of organic pollutants

Particle size and shape could affect the rate of reactions because this affects the size of the bandgap and the diffusion length of photoproduced charge carriers from the bulk to the surface-active sites. The size of the bandgap energy in turn determines the photonic efficiency and the range of wavelengths of the electromagnetic radiation to be harvested during the degradation reactions. To maximize pollutants eradication, the bandgap should not be too small (<1.3 eV) to minimize the high probability of charge carriers recombination nor be too large (>3.0 eV) to be activated in the visible region of the electromagnetic spectrum and as such a bandgap in the range of 1.3–3.0 eV has generally been reported to be appropriate for photocatalytic degradation reactions (Imtiaz et al., 2019). Pure CuO has a bulk bandgap of 1.2 eV and this value could reach up to 3.57 eV in the nanoscale size regime by adjusting synthesis methods (Mallick and Sahu, 2012). However, one of its main drawbacks, when used as a photocatalyst, is the high degree of e^-/h^+ pairs recombination owing to its CB edge potential being more positive than the redox potential of hydrogen, which results in reduced catalytic activity (Nuengmatcha et al., 2019). As a consequence, its catalytic activity has been boosted via doping with other elements or coupling with other semiconductors because of the resulting enhanced features such as surface area and adsorption capacity better mobility and separation of charge carriers.

Several researchers studied the influence of particle size and shape on the degradation performance of CuO and CuO-based photocatalysts for various organic contaminants. For instance, Muthuvel *et al.* (Muthuvel et al., 2020) found enhanced catalytic activity of CuO NPs with an average particle size of 25 nm as compared to 32 nm-sized spherical particles synthesized by chemical and biological methods, respectively towards methylene blue degradation under

similar experimental conditions. In a study conducted by Junior *et al.* (Junior et al., 2019) for the degradation of the same dye using CuO NPs with different morphologies, the decomposition performance was found to increase in the order of plate-like > flower-like, boat-like > ellipsoidal like CuO particles at comparable experimental setting. Similarly, a comparison of the degradation capability of CuO nanorods, nano leaves, and nanosheets for Congo red employing the same catalyst dose of 50 mg, 100 mL of 20 ppm dye concentration under 18W UV lamp for 210 minutes showed that the particles achieved respective degradation efficiency of 67, 48, and 12% (Sadollahkhani et al., 2014). According to the authors, the observed efficiency disparity was attributed to the greater adsorption capacity arising from the higher specific surface area of the former particles than the latter. In another report by Nazim *et al.* (Nazim et al., 2021), the degradation competence of porous CuO nanosheets for the food dye Allura red AC was 97% in 6 minutes in the presence of $NaBH_4$ (1 mg/mL) under UV light irradiation and starting with 10 mL of 5 ppm dye concentration and 5 mg of CuO catalyst, which was much higher than other CuO NPs morphologies compared. This higher catalytic activity response of the CuO nanosheets to the degradation of the dye was ascribed to the greater surface area and adsorption ability of the catalyst nanosheets and also due to the augmented production of $HO^{\cdot}$ radicals via reduction of O_2 to $O_2^{-\cdot}$ and then to $HO^{\cdot}$ with electrons supplied by $BH_4^{-\cdot}$ in the reaction medium. In another study, a comparison of the photocatalytic activity of as-synthesized CuO and Tb-doped CuO for the catalytic degradation of MB for 2h showed that the latter improved the efficiency by 6% compared to the former (Vimala Devi et al., 2017). This was attributed by the authors for two reasons. The first reason for the enhancement was proposed to be due to the smaller particle sizes of the Tb-doped CuO in which faster diffusion of charge carriers to the surface is facilitated, resulting in the generation of more reactive radicals and hence faster removal efficiency. The second reason was

ascribed to the effective separation of photogenerated charge carriers by the presence of more surface defects on Tb-CuO which serve as electron trapping centers as well as the presence of Tb^{3+} ions on the surface, acting as VB electron traps to produce Tb^{2+} and $O_2^{-\cdot}$.

One bottleneck for effective catalytic activity with narrow band gap semiconductors such as CuO is the high chance of photogenerated e^-/h^+ pairs recombination and this can be alleviated via elemental doping, defect formation, morphology and size control or coupling it with other semiconductors (Fang et al., 2021). Sasikala *et al.* (Sasikala et al., 2016) investigated the photocatalytic activity response of Ce-loaded CuO NPs for the degradation of trypan blue dye and found greater activity than pure CuO NPs. This enhancement was ascribed to the facilitated separation of photogenerated e^-/h^+ pairs due to Ce atoms serving as CB electron traps, Figure 7. Moreover, the removal of Congo red dye with Cd, Ba-CuO was reported to be higher than Cd-CuO, Ba-CuO, and undoped CuO nanoparticles (Arunadevi et al., 2018). It was found that Cd, Ba-CuO degraded the dye by 98% for 3h degradation reaction time under visible light irradiation, an improvement by about 25% compared to undoped CuO under similar experimental settings. The higher removal efficiency of the Cd, Ba-CuO was ascribed to the inhibition of photogenerated e^-/h^+ pairs recombination by the Cd and Ba impurities forming intraband energy levels near the CB or the VB of CuO and narrowing the effective bandgap and serving as CB electron sinks, thereby promoting redox reactions to produce a large number of reactive radicals which are responsible for the destruction of dye molecules. However, elemental doping does not necessary result in an increment of activity of the metal oxides rather it could have the opposite effect. A case in point is the slight reduction observed in the degradation of methylene blue using 6% Fe-doped CuO film with degradation of 94.9% as compared to 95.6% using CuO film for a 12h solar irradiation as reported by Sayed and Shaban (El Sayed and Shaban, 2015). The authors suggested

that the higher bandgap (2.30 eV) of 6%Fe-doped CuO film than the bandgap of pure CuO film (2.15 eV) might have caused less photons to have induced photoexcitation and formation of reactive $HO^{\cdot}$ radicals and reduced rate of degradation.

The presence of surface defects such as oxygen vacancy and oxygen excess, edges or corners formed during synthesis in CuO NPs can also act as trapping sites for photogenerated charge carriers, resulting in their improved separation and transfer and enhanced rate of reactive radicals generation and pollutant removal proficiency (Katal et al., 2020; Hasija et al., 2021a). However, a large population of defects in CuO can hamper the mobility of charge carriers and serve as recombination centers and result in a hindered rate of decomposition (Sharma et al., 2016; Katal et al., 2020).

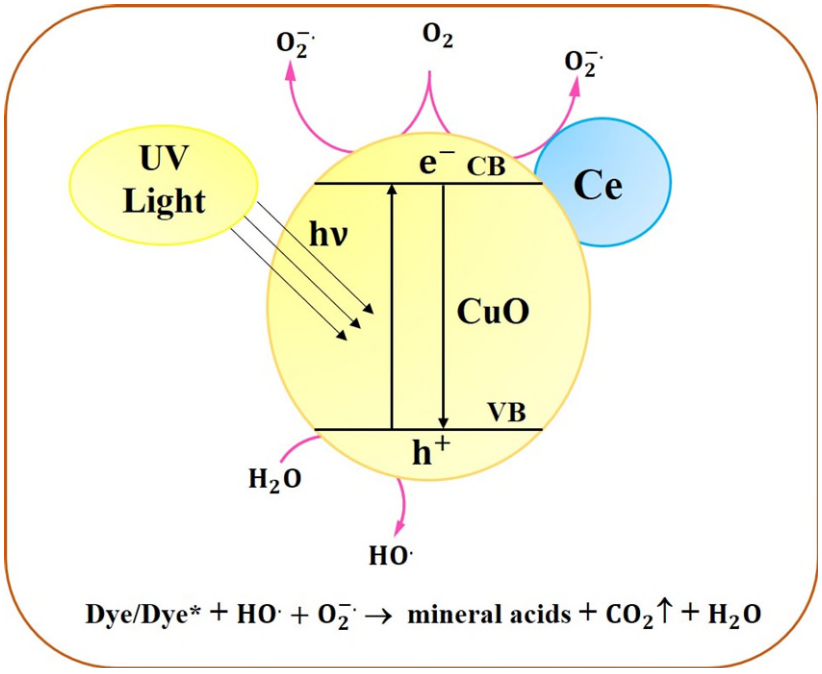

Figure 7. Photocatalytic degradation mechanism of trypan blue dye using Ce/CuO NPs (Sasikala et al., 2016).

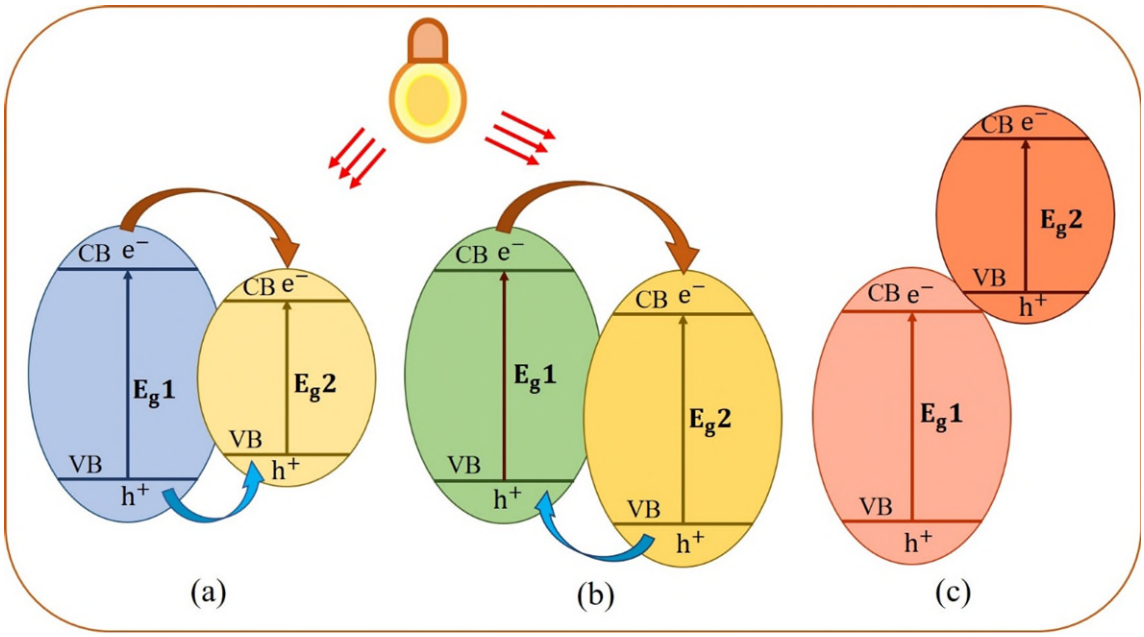

Figure 8. Possible bandgap alignment, (a) straddling band gap, (b) staggered gap, and (c) broken gap of semiconductors 1 and 2 with their respective energies, E_g1 and E_g2.

Another method of inhibiting the recombination rate of e^-/h^+ pairs in CuO are to couple it with other semiconductors with proper band gap alignment to form heterojunctions. Depending on the CB and VB potential alignments with other semiconductors, there can be three possible types of band gap intercalations. These include staggering gaps, straddling gaps, and broken gaps as illustrated in Figure 8. While in straddling bandgap alignment both CB electrons and VB holes are transferred from the wider semiconductor 1 to the narrower bandgap semiconductor 2, Figure 8 (a), in staggered gap CB electrons from semiconductor 1 with more negative potential are transferred to CB of semiconductor 2 and VB holes move in the opposite direction, Figure 8 (b). On the other hand, in broken gap configuration, Figure 8 (c), both CB electrons and VB holes of semiconductor 2 are more negative than semiconductor 1 and no charge carrier transfer from one semiconductor to the other can occur across the interface between them because of energy barrier and of the three possible bandgap alignments mentioned, type II (staggered bandgap alignment) results in better separation of charge carriers and higher degradation percentage (Koe et al., 2020).

Several studies reported on the photocatalytic proficiency of CuO-based type II heterojunctions for organic contaminants. For example, Mageshwari *et al.* (Mageshwari et al., 2015) reported enhanced photocatalytic performance of CuO/ZnO composite for methyl orange and methylene blue dyes as compared to pure CuO and ascribed this improved performance of the composite to the enhanced charge transport and efficiency of charge carriers separation owing to intercalated band gap positions by the n-type ZnO and p-type CuO (n-p) heterojunction formation between the two oxides, Figure 9 (a), which prolongs the lifetime of photogenerated e^-/h^+ pairs and the formation of more reactive radicals and higher removal efficiency. In another study reported by Hossain *et al.* (Hossain et al., 2020) it was observed that the catalytic activity of CuO/CdS nanocomposite for the photocatalytic degradation of rhodamine B was superior (93%) as compared to the performance achieved by the individual phases of CuO and CdS which degraded the dye by 41 and 60%, respectively under the same experimental condition of initial dye concentration 30 ppm and catalyst dose of 0.25 g/L for 1 h of irradiation under visible light. The authors have reasoned the greater performance of CuO/CdS heterostructures photocatalyst than the individual phases to be owing to efficient photogenerated charge carrier separation, accelerated charge carrier transfer across the surface/solution interface, and its higher BET specific surface area. The photocatalytic degradation mechanism is shown in Figure 9 (b).

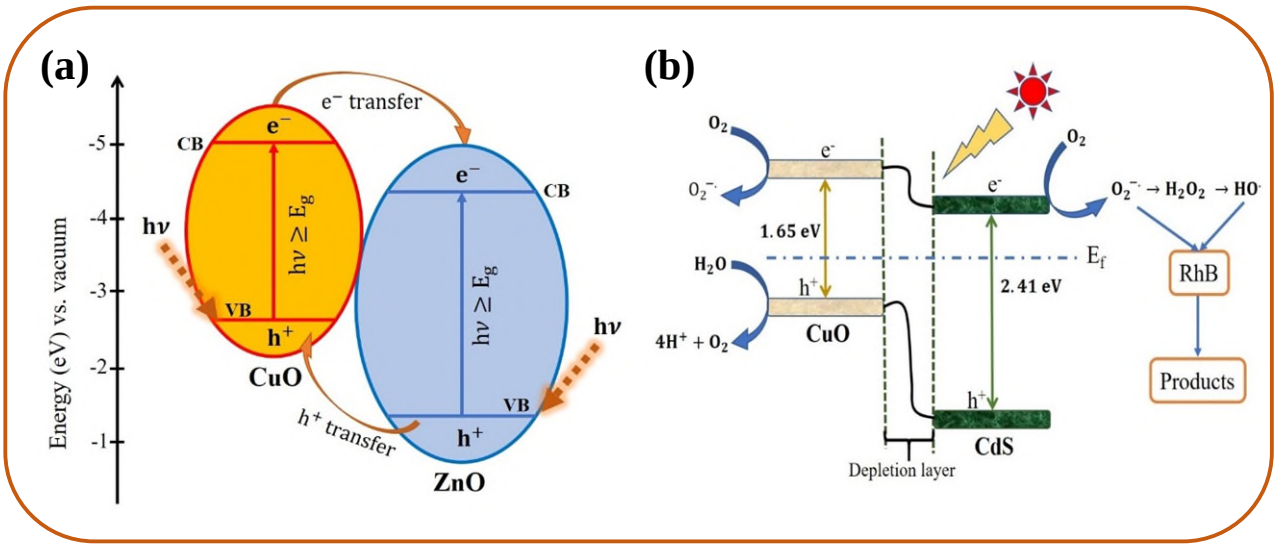

Figure 9. Illustration of e^-/h^+ formation and separation in CuO/ZnO composite (a), reprinted with permission from reference (Mageshwari et al., 2015). Copyright 2014. Elsevier, (b) RhB using CuO/CdS p-n heterojunction catalyst. Reprinted with permission from reference (Hossain et al., 2020). Copyright 2020. Elsevier.

However, a Z-scheme charge transfer mechanism was proposed for the observed enhanced photocatalytic activity of CuO-WO_3 heterojunction catalyst for the degradation of methylene blue dye as compared to the degradation efficiency achieved by bare WO_3 NPs (Dursun et al., 2020). Here, the type II heterojunction mechanism is not able to explain the phenomena because CB electrons in WO_3 cannot reduce O_2 to $O_2^{-\cdot}$ As the reduction potential for $O_2/O_2^{-\cdot}$ is more negative than the CB edge potential of WO_3 and VB holes in CuO cannot oxidize H_2O to $HO^{\cdot}$ because VB edge potential is more negative than the oxidation potential of $HO^{\cdot}/H_2O$, as clearly indicated by the red-crossed "X" symbol in Figure 10. One advantage of the Z-scheme heterojunction over type II heterojunctions is that unlike in type II, it results in effective charge carriers separation while maintaining the redox ability of the composite because, during the transfer process, the reducing ability of CB electrons in the semiconductor with more negative potential and the oxidizing ability of the VB holes in the semiconductor with the more positive potential is not affected (Wang et al., 2020a). Therefore, Z-scheme heterojunctions avoid the drawback of reducing the redox potential

during the charge transfer process observed in type II heterojunctions while maintaining the charge carrier separation efficiency. Similarly, a Z-scheme charge transfer mechanism was proposed for the enhanced visible-light-driven photocatalytic degradation of malachite green (MG) using CuO/g-C_3N_4 catalyst as compared to the pure semiconductors (Tzvetkov et al., 2019).

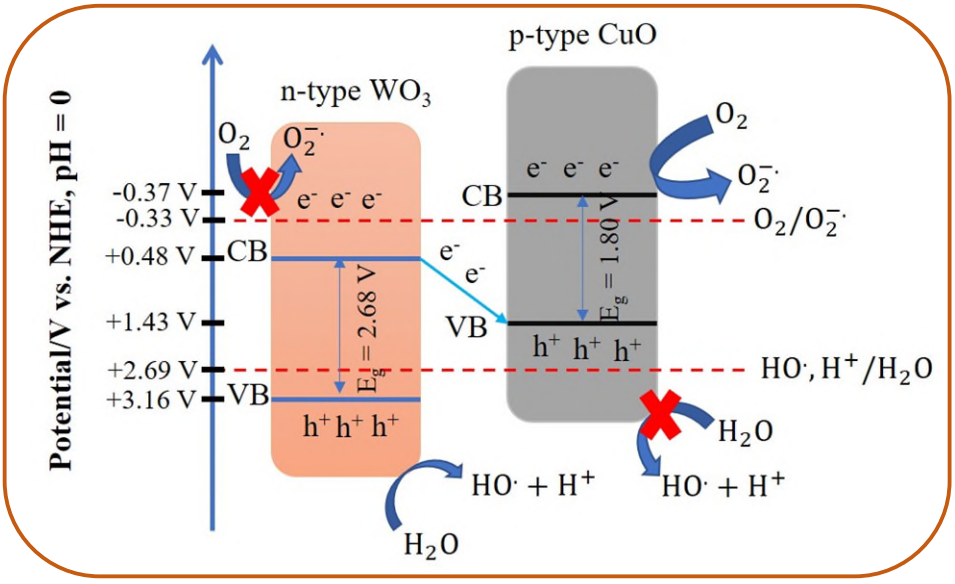

Figure 10. Electron transfer mechanism during the degradation of methylene blue using WO_3-CuO n-p heterojunction catalyst. Adapted from reference (Dursun et al., 2020).

In this mechanism, VB electrons from semiconductors g-C_3N_4 and CuO are excited to their respective CB and the CB electrons in CuO move to the VB of g-C_3N_4 at the interface, and CB electrons in g-C_3N_4 reduce dissolved oxygen to $O_2^{-\cdot}$ Radical meanwhile VB holes in CuO oxidize H_2O or HO^- to $HO^\cdot$ radical, resulting in effective separation of e^-/h^+ pairs and generation of numerous reactive radicals and a higher destruction rate of the MG molecules, Figure 11 (a). In addition to binary composites, researchers have also synthesized ternary composites to boost the photocatalytic degradation of different organic contaminants. For instance, Kumaresan *et al.* (Kumaresan et al., 2020) noticed that the photocatalytic activity of reduced graphene oxide (rGO)-based CuO/ZnO that is CuO/ZnO/rGO ternary composite exhibited catalytic activity 12 times

519 more than that achieved by CuO/ZnO binary composite towards Rhodamine B (RhB) dye under
520 visible light irradiation and explained that the pronounced degradation of the ternary composite
521 compared to the binary composite is due to the excellent adsorption and charge carriers conducting
522 properties of the rGO in the composite. It has also been reported that the greater decomposition
523 rate of the antibiotic tetracycline hydrochloride using rGO/CuO/Cu_2O catalyst compared to the
524 pure phases was due to the presence of rGO which boosts the stability of CuO/Cu_2O catalyst and
525 also acts as CB electron acceptor thereby facilitating the separation of e^-/h^+ pairs and production
526 of more reactive radicals and higher degradation rate (Bai et al., 2021), Figure 11(b).

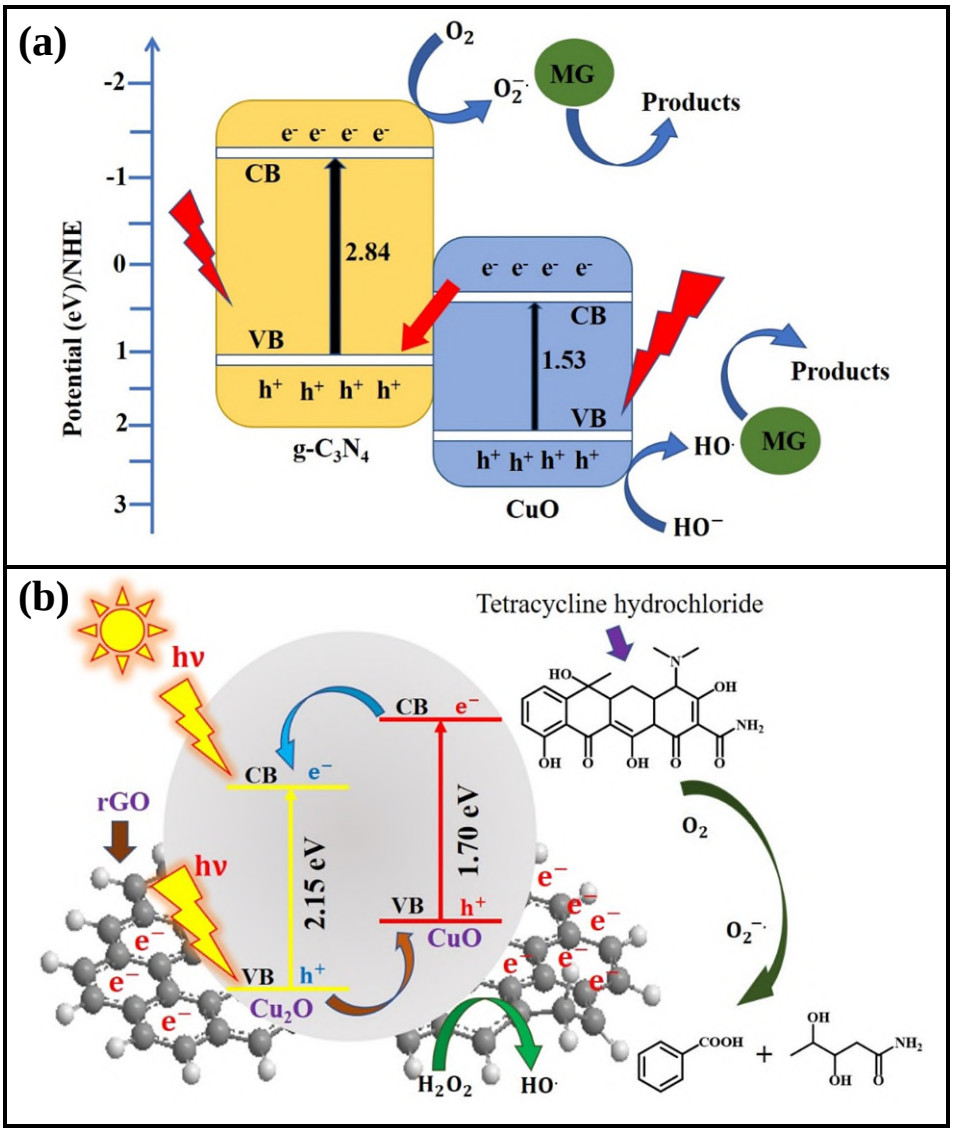

527 **Figure 11.** Band gap position and electron transfer mechanism in the degradation of (a) CuO/g-C_3N_4
528 composite (Tzvetkov et al., 2019) (b) Tetracycline hydrochloride using rGO/CuO/Cu_2O catalyst. Reprinted
529 with permission from reference (Bai et al., 2021). Copyright 2021. Elsevier.

530 Bajiri *et al.* (Bajiri et al., 2019) studied the photocatalytic performance of CuO/ZnO/g-C_3N_4
531 ternary composite for the photocatalytic degradation of methylene blue under visible light
532 illumination. In this Z-scheme mechanism, the photogenerated CB electrons in ZnO transfer and
533 combine with holes in g-C_3N_4 and CuO, leaving holes in the VB. Then, the VB holes can oxidize
534 HO^- to $HO^{\cdot}$ because they have enough potential (3.0 V) compared to the potential needed to

produced $HO^{\cdot}$ (1.99 V vs. NHE at neutral pH). Moreover, the CB electrons of CuO and g-C_3N_4 are also capable of reducing O_2 to $O_2^{-\cdot}$ Because their respective redox potential -0.77 V and -1.12 V are enough to produce $O_2^{-\cdot}$ Radicals (-0.046 V). Thus, they reasoned that the enhanced photocatalytic activity of the ternary composite for the organic pollutant is best explained by the Z-scheme mechanism.

In another study by Liu *et al.* (Liu et al., 2012), the higher degradation of RhB using CuO nanoflower (NF)-decorated rGO than pure CuO under UV irradiation in the presence of H_2O_2 oxidant was because of the facilitated adsorption of RhB by π-π stacking interactions between RhB and the π-conjugation system of CuONF/rGO, leading to the fast degradation of the dye. Similar higher catalytic activity for 4-nitrophenol and 2-nitrophenol pollutants using CuO/rGO catalyst than pure CuO NPs was also reported and the reason had been attributed to the good photoexcited electron capturing ability of the graphitic backbone and also the good transfer of charge carriers, resulting in efficient separation of charge carriers and higher reactive radicals and rate of reaction (Botsa and Basavaiah, 2018), Figure 12. Additionally, Dutta *et al.* (Dutta et al., 2016) found 99% degradation of methylene blue using CuO quantum dots decorated rGO in the presence of H_2O_2 in 50 minutes of irradiation under visible light. According to the authors, the enhanced degradation of the dye is due to excess formation of $HO^{\cdot}$ and $O_2^{-\cdot}$ Reactive radicals' production by the visible-light-induced excitation of electrons from rGO and transferring to the CB of CuO, resulting in more radicals' production and improved degradation reaction rate. Similar enhanced removal of methylene blue and Congo red dyes using rGO-CuO catalyst under visible light illumination was also recently reported by our group (Sagadevan et al., 2021).

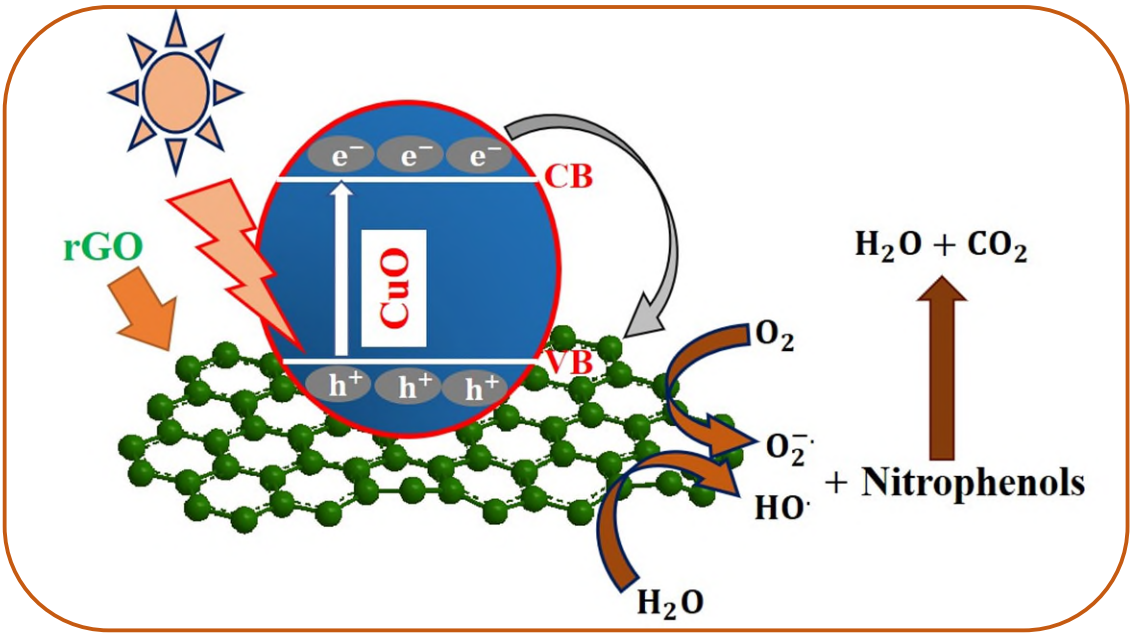

Figure 12. Illustration of electron transfer mechanism in CuO/rGO composite during the degradation of RhB dye. Adapted from reference (Botsa and Basavaiah, 2018).

Similar to elemental doping, coupling CuO with other semiconductors may not necessarily result in enhanced photodegradation rather consideration of other factors such as resulting bandgap and surface area of catalyst need to be taken into consideration to explain the experimentally observed degradation efficiency. For example, in a study reported by Koohestani (Koohestani, 2019), the degree of elimination of methyl orange using pure CuO NPs was found to be higher than Cu_2O/CuO composites. According to the author, this could be due to the smaller bandgap and larger specific surface area of CuO NPs than the Cu_2O/CuO photocatalyst.

2.1.5.2 Effects of type of catalyst and organic pollutant on degradation efficiency

The photocatalytic degradation percentage of organic contaminants in aqueous media is potentially influenced by the nature of the catalyst as well as the organic contaminants keeping other variables unchanged. The photocatalytic activity response of a given catalyst to different pollutants can vary depending on the nature of the pollutants. This variation may generally be

attributed to disparity in molecular mass, molecular structure and stability, and molecular charges at the pH of the reaction suspension. Several researchers have reported the performance of CuO and CuO-based catalysts for the photocatalytic destruction of various organic contaminants. For example, Singh *et al.* (Singh et al., 2017) studied the catalytic activity of CuO nanorods synthesized by sol-gel method to the degradation of methyl orange, methylene blue, Eriochrome Black T, and Congo red dyes individually and under similar experimental conditions and they found removal percentages in increasing order: Congo red < methylene blue < Eriochrome Black T < methyl orange. This observed discrepancy of degradation performance of the same catalyst to Congo red (M_w = 696.7 g/mol) with the slowest rate of degradation as opposed to methyl orange (M_w = 327 g/mol) with the highest rate was attributed to their variation in molecular mass of the dyes which results in different diffusion rate to catalyst surface active sites and hence the rate of decomposition reaction. In another study, the extent of degradation of Nile blue was found to be 97% while that of reactive yellow 160 was 80% under sunlight irradiation for 2 h utilizing the same biosynthesized CuO NPs catalyst (Singh et al., 2019). A similar explanation that is based on the variation in the diffusion rate to catalyst surface active sites owing to the difference in molecular mass and structure of the dye molecules was offered to the observed disparity in catalytic performance. Moreover, methylene blue was degraded by 39% as compared to 28% for methyl orange under visible light irradiation for a period of 2h using the same ZnO/CuO (50:50) photocatalyst (Saravanan et al., 2013). In a study conducted by using the same 10 ppm pollutant concentration for 320 minutes of irradiation under sunlight at their respective natural pH and catalyst dose of 10 mg/L of biosynthesized CuO NPs for six different pollutants of methyl red, Congo red, methylene blue, trypan blue, methyl orange, and Coomassie brilliant blue, the respective degradation percentages obtained were 77.4, 77.7, 79.6, 72.04, 59.9, and 43.6 %

(Yugandhar et al., 2019). In a different investigation, a comparison of the degradation of methylene blue, methyl red and Congo red dyes taken individually using electrochemically synthesized CuO NPs and a similar amount of catalyst and dye concentration under sunlight illumination for a period of 2h resulted in degradation of 93, 90, and 85%, respectively (Katwal et al., 2015). The rate constant of the reactions was different with the highest value of 0.02059 min^{-1} belonging to the degradation of methylene blue and the lowest 0.01749 min^{-1} for Congo red and the authors have explained the observed lowered rate of degradation of Congo red are due to its less susceptible chemical structure to oxidation and also steric hindrance originating from the biphenyl group and naphthenic groups in its structure.

Nevertheless, the explanation by molecular mass difference alone may not necessarily account for the experimentally observed difference in the removal efficiency of dyes employing the same catalyst. For example, it has been reported by Hossain *et al.* (Hossain et al., 2020) that the removal percentages of rhodamine B, methylene blue, methyl blue, and methyl orange dyes utilizing CuO/CdS composite catalyst were 93%, 75%, 83%, and 80%, respectively with molecular masses which is 479, 319.85, 800, and 327 g/mol, respectively. Thus, other factors such as molecular structural complexity and stability including the ionicity of the molecules at the experimental pH should also be taken into consideration to account for the observed variation in degradation competence.

The elimination rate of a given organic pollutant using CuO and CuO-based catalysts also depends on the type of catalyst. This could be primarily a result of the associated variation in band gap energy, particle morphology, specific surface area, the efficiency of photogenerated charge carrier separation as discussed previously. A case in point is the degradation of phenanthrene using $Gd_2O_2CO_3$/CuO/ZnO nanocomposite exhibited a higher removal rate of 99.6 % during 2h of

illumination time under visible light as compared to 50.4% when pure CuO was used for the same time duration (Mukwevho et al., 2019). This enhanced performance of the ternary nanocomposite was attributed to its high light absorption, high surface area, and reduced recombination rate of charge carriers. Moreover, the degradation rate of methylene blue and methylene violet dyes taken separately using Zn-doped CuO nanoflowers was higher than utilizing pure CuO nanorods at comparable other experimental parameters (Sonia et al., 2015b). It has been suggested that the enhanced activity of the Zn-doped CuO relative to the pure CuO was because of the efficient separation of photogenerated e^-/h^+ pairs as a result of the Zn atoms acting as CB electron traps and a hence results in the larger number of reactive radicals' production and degree of removal of the dyes.

2.1.5.3 Effects of catalyst dose and pollutant initial concentration

The initial catalyst dose and pollutant concentration employed are among the operational parameters that affect the removal efficiency of organic pollutants. Generally, heterogeneous photocatalytic reactions are effective at the optimal amount of catalyst dose and dye concentration. Regarding pollutant concentration, photocatalytic reactions are efficient at lower concentrations because higher concentrations prevent radiation penetration and obscure catalyst active sites thereby minimizing the number of reactive radical species that would have been produced and hence suppress the rate of the degradation process. Similarly, using a catalyst amount above optimal could form a suspension that occludes radiation from passing through and fosters particle agglomeration which in turn tends to reduce the number of active surface sites and the rate of the decomposition process. Utilizing the below optimal amount of catalyst will also decrease the extent of degradation for a lower number of surface-active sites for the formation of reactive species will be produced. Thus, the influence of dye initial concentration and catalyst dose on the

640 removal efficiency of pollutant compounds are among the important operational parameters that
641 are studied and optimized in many photocatalytic degradation reactions. To mention some,
642 Venkata *et al.* (Venkata et al., 2019) studied the impact of varying the initial concentrations of
643 Coomassie Brilliant Blue R-250 and methylene blue dyes separately from 5 to 25 ppm in intervals
644 of 5 ppm employing a fixed catalyst loading of 10 mg and pH of 7 under sunlight irradiation. They
645 observed that the degradation decreased with a rise in dye concentration in both dyes and attributed
646 this phenomenon to increased coverage of surface-active sites with dye molecules, resulting in a
647 reduced rate of reactive species production and hence decomposition. Moreover, the authors also
648 observed that increasing catalyst dose from 5–25 mg keeping other variables fixed resulted in
649 respective maximum degradation percentages of 74 and 86% but any further addition of the
650 catalyst above 25 mg lowered the degradation. This has been ascribed to particle aggregation and
651 solution turbidity which result in a reduction in surface active sites and blockage of radiation,
652 respectively and hence lower destruction of the dyes. Akram *et al.* (Akram et al., 2020) studied the
653 effect of $Co(OH)_2$/CuO catalyst dose by varying from 5–20 mg in intervals of 5 mg and rhodamine
654 B dye initial concentration from 25–100 mg/L in intervals of 25 mg/L on the percentage of
655 degradation and found maximum value of 99.9% at 10 mg catalyst dose and 25 mg/L dye initial
656 concentration. Keeping other experimental parameters unchanged, increasing catalyst loading
657 above 10 mg or dye initial concentration above 25 mg/L hindered degradation probably because
658 both cases result in scattering or obstruction of radiation which in turn results in ineffective
659 production of reactive radicals and lowered rate of degradation. In another study reported by Date
660 *et al.* (Date et al., 2020), the photocatalytic performance of CuO/TiO_2 hybrid nanorod arrays was
661 consistently decreased with an increase in rhodamine B initial concentration from 50 to 250 and
662 then to 750 ppm in the presence of H_2O_2 oxidant and without varying other experimental

parameters. According to the authors, the enhanced activity of the hybrid photocatalyst relative to bare CuO was due to the formation of type II heterostructures between CuO and TiO_2, which results in more efficient separation of charge carriers and the formation of more $HO^{\cdot}$ and $HOO^{\cdot}$ radicals generated from H_2O_2 via its reaction with photogenerated e^-/h^+ pairs in a process called photo-Fenton-catalysis and therefore a greater degradation rate. Similarly, the influence of Direct red 89 initial concentration on the photocatalytic activity of Fe_3O_4/CuO core-shell heterostructures under visible light irradiation was studied by Benabbas *et al.* (Benabbas et al., 2021). They found that nearly complete removal of the dye was achieved utilizing its initial concentration in the range from 20 – 60 ppm and catalyst dose of 0.75 g and 100W visible light irradiation at the experimental pH of 6 for 240 min. However, degradation decreased upon increasing the initial concentration from 40 – 60 ppm while other parameters are kept fixed. As mentioned previously, the authors have reasoned this to be due to suppressed rate of radical formation as a result of coverage of catalyst surface active sites by dye molecules at higher concentration as well as radiation screening effect of dye molecules, both of which result in reduced generation rate of radicals and rate of degradation reaction. A consistent reduction in the rate of destruction of methylene blue up on increasing its initial concentration from 5 to 20 ppm using CuO/ZnO nanocomposite catalyst was also reported by Sakib *et al.* (Sakib et al., 2019). In a study reported by Abdullah *et al.* (Abdullah et al., 2016) for the photocatalytic degradation of methylene blue using CuO-$BiVO_4$ catalyst, while the percent of decomposition of the dye monotonically lowered with the rise in its concentration from 10 to 30 ppm in intervals of 5 ppm without changing other experimental variables, the degradation increased and reached maximum value upon increasing catalyst dose from 0.2 to 0.8g in intervals of 0.2 g but further increment above 0.8 to 1 g did not change significantly. Table 1 provides additional examples of degradation efficiency achieved by CuO and CuO-based

686 photocatalysts for the degradation of different organic pollutants at the indicated experimental
687 parameters as reported from various references.

688 **Table 1.** Effects of catalyst dose and pollutant initial concentration on the photocatalytic removal efficiency
689 of various organic pollutants in an aqueous solution. [Pollutant] = initial concentration of pollutant.

Pollutant	[Pollutant] (ppm)	Catalyst	Catalyst dose (g)	Conditions	D (%)	Ref.
4-Nitrophenol	10	CuO/rGO	0.03	pH = 8.1, t = 2 h, under visible light	100	(Botsa and Basavaiah, 2018)
4-Nitrophenol	10	CuO	0.03	pH = 8.1, t = 2 h, under visible light	72	(Botsa and Basavaiah, 2018)
Acid Fuchsin	20	CuO/MnO_2	Single film	V = 3 mL, 0.05 mL H_2O_2, 0.45 mL H_2O, t = 8h,	94.1	(Yang et al., 2014)
Methylene blue	10	1wt% $CuO-BiVO_4$	0.8	V = 1L, pH = 10, t = 4h, under 18W visible light	100	(Abdullah et al., 2016)
Rhodamine B	0.0105	$Co(OH)_2/CuO$	0.02	V = 50 mL, pH = 7, t = 8 min., using UV light	99.9	(Akram et al., 2020)
Methylene blue	10	CuO/Co_3O_4	---	V = 50 mL, t = 3h, using 500 W Xe lamp	56	(Chen et al., 2015)
Methylene blue	10	CuO	---	V = 50 mL, t = 3h, using 500 W Xe lamp	40	(Chen et al., 2015)
Methylene blue	40	CuO/MgO	1.0	V = 100 mL, pH = 2.2, t = 80	96	(Priya et al., 2019)

				min., using UV light		
Phenanthrene	20	$Gd_2O_2CO_3$/ZnO/CuO	0.4 g/L	V = 100 mL, pH = 4, t = 2 h, using visible light	99.6	(Mukwevho et al., 2019)
Methylene blue	15	0.07M Zn-CuO	0.005	t = 3 h, using visible light	~ 100	(Sonia et al., 2015a)
Methylene violet	15	0.07M Zn-CuO	0.005	t = 3 h, using visible light	~ 100	
Methylene blue	100	Ag@CuO/PAA	0.1	V = 100 mL, t = 30 min, under sunlight	99.0	(Iqbal et al., 2020)
Rhodamine B	10	CuO/Fe_2O_3	0.04	V = 80 mL, t = 1hr,	100	(Alp et al., 2019)
Direct red 89	20	Fe_3O_4/CuO	0.75	V = 250 mL, 7 mL H_2O_2 added, t = 240 min., using 100W visible lamp	~ 100	(Benabbas et al., 2021)
Aniline	100	CuO	0.05 g/L	t = 1 h, pH = 7, using 30W UV-C lamp	78	(Norzaee et al., 2017)
Congo red	10	1wt%CuO/eggshell	1 g/L	t = 4h under visible light	80	(Fahmi Khairol et al., 2019)
Bisphenol A	20	BiOCl/CuO	50 mg	t =1 h using 600W xenon lamp	93.43	(Li et al., 2019)
Acid orange	20	BiOCl/CuO	50 mg	t =1 h using 600W xenon lamp	98.42	

690

2.2 Photocatalytic activity of CuO NPs for removal of toxic metal ions

In addition to organic pollutants, inorganic pollutants are also common in discharged effluents from various industries. These include heavy metals, sulfates, cyanides, mineral acids, etc and can pollute water if available in higher than permissible limits (Wasewar et al., 2020). Removal of toxic heavy metal ions is crucial to ensure their safety to humans and the environment. Heavy metal ions such as Ni (II), Hg (II), Pb (II), As (III), Cd (II), Cr(VI) are among the contaminants listed under priority pollutants by the United States Environmental Protection Agency (USEPA), and as such a maximum allowable limit of these ions in wastewater, soil for agriculture, and drinking water has been stipulated by different organizations. For instance, the World Health Organization (WHO) has set recommended safe concentration limit of some heavy metals such as Hg (II), Cd^{2+}, Pb (II), Cr (VI), and Ni^{2+} in wastewater equal to 0.001, 0.003, 0.01, 0.05, and 0.02 ppm, respectively (Kinuthia et al., 2020a). Since consumption of these metal ions from different sources in humans can induce multifarious health problems principally by replacing the nutritional metals of organic cells in our body and inhibiting their function and also dysfunction our vital organs such as kidney, liver, nervous system, the brain function and could even cause death they should be controlled and managed and removed from their sources mainly those effluents from industrial wastewater to meet stringent discharge standards (Le et al., 2019a). Moreover, metal ions are not biodegradable and discharges of low concentration of these ions can lead to their enrichment over long-term accumulation via the food chain and drinking water and therefore heavy metal ion recovery via photocatalytic reduction may be the best option to address the specified problems (Wenten et al., 2020; Ren et al., 2021). Photocatalytic reduction is also one alternative approach for recovering precious metals such as platinum, silver, and gold from wastewater effluents. Table 2 gives the most common toxic heavy metal ions with the toxicity they induce to

714 humans and the environment as well as the toxicity limit set by different organizations in
715 agricultural soils, drinking water, and industrial effluents.

716 These metal ions are to be reduced to an elemental or lower valency state by the CB electrons of
717 the semiconductor, the reduction potential of the metal should be more positive than the CB edge
718 potential of the semiconductor being used. The standard reduction potential of the most toxic metal
719 ions and metalloid arsenic ion in water at 25 °C vs NHE is given in Eq. (20-25).

720 $$Pb^{2+}(aq) + 2e^- \rightarrow Pb(s) \qquad E^0 = -0.13\ V \qquad (20)$$

721 $$Hg^{2+}(aq) + 2e^- \rightarrow Hg(l) \qquad E^0 = +0.85V \qquad (21)$$

722 $$Cd^{2+}(aq) + 2e^- \rightarrow Cd(s) \qquad E^0 = -0.40\ V \qquad (22)$$

723 $$Ni^{2+}(aq) + 2e^- \rightarrow Ni(s) \qquad E^0 = -0.26\ V \qquad (23)$$

724 $$H_3AsO_4(aq) + 2e^- \rightarrow H_3AsO_3(aq) \qquad E^0 = +0.56\ V \qquad (24)$$

725 $$Cr_2O_7^{2-}(aq) + 14H^+(aq) + 6e^- \rightarrow 2Cr^{3+}(aq) + 7H_2O; \quad E^0 = +1.33\ V \qquad (25)$$

726 Similarly, for the metal ions to be oxidized to a higher valence state, the oxidation potential of
727 photogenerated holes should be more positive than the oxidation potential of the metal ions. For
728 example, Pb^{2+} has been removed by reacting with available HO^- forming $Pb(OH)_2$ precipitates or
729 getting oxidized to PbO_2 via reaction with h^+ or $HO^{\cdot}$ and reacting with dissolved O^{2-} thereby
730 changing its oxidation state to Pb(IV), Eq. (26) (Le et al., 2019b).

731 $$Pb^{2+} \rightarrow Pb^{4+} + 2e^- \qquad E^0 = -0.67\ V \qquad (26)$$

732 Chromium (Cr) can exist principally in hexavalent Cr(VI) or trivalent Cr(III) oxidation states in
733 soils and aqueous environment and while Cr(VI), which exists in CrO_4^{2-} and $Cr_2O_7^{2-}$ is toxic,
734 cancerogenic and mutagenic contaminant, Cr(III) is vital micronutrient for the human body (Wang

et al., 2020b; Wang et al., 2022). Therefore, reducing the oxidation state from VI to III is a safe method used to avoid the toxicity associated with chromium compounds in aqueous media. Similar to chromium, arsenic primarily occurs in arsenite (As (III)) and arsenate (As(V)) oxidation states of which As (III) is the prevalent form it exists in groundwater and is much more toxic than As (V) and as such one viable option to avoid its toxicity will be to oxidize it to its less toxic oxidation state (Sharma and Sohn, 2009).

Several reports in the literature emphasized the photocatalytic reduction of toxic heavy metal ions using CuO and CuO-based photocatalysts. For example, almost complete reduction of chromium from Cr(VI) to Cr(III) valence state has been achieved via photoreduction using the mesoporous CuO/ZrO_2-MCM-41 nanocomposite catalyst in 30 minutes (Nanda et al., 2017). In another study, 100% photoreduction of 100 ppm of Cr(VI) to Cr(III) was achieved using TiO_2/rGO/CuO ternary composite as photocatalyst in 80 minutes under visible light irradiation (Wang et al., 2020b). The photocatalytic reduction of Cr(VI) using CuO nanoparticles together with different organic acids under simulated solar illumination was also reported (Li et al., 2017).

Table 2. List of toxic heavy metal ions, their maximum contaminant level as set by different organizations and their toxicity. [a] = USEPA; [b] = WHO; [c] = European Union (EU).

S/N	Heavy metal ion	Maximum concentration limit (mg/L)			Toxicity	Ref.
		Drinking water	Agriculture soils	Wastewater		
1	Hg^{2+}	0.002[a], 0.001[c]	0.050[b]	0.00003[a], 0.001[b], 0.005[c]	Kidney disease, disease of circulatory and nervous system	(Tran et al., 2017; Ahmad et al., 2020)

2	Pb^{2+}	0.015[a], 0.010 [b, c]	0.100[b]	0.006[a], 0.010[b]	Digestive problems, high blood pressure, kidney, circulatory, and nervous system diseases, memory problem in adults	(Contreras Rodríguez, 2015; Ahmad et al., 2020)
3	Cd^{2+}	0.005[a, c], 0.003[b]	0.003[b]	0.010[a], 0.003[b]	Human carcinogen, kidney, renal, cardiovascular, central and peripheral system, reproductive and respiratory system damage	(Tran et al., 2017; Ahmad et al., 2020)
4	As^{3+}	0.010[b],	---	0.050[a]	Causes cancer in skin, lung, and bladder	(Mahmud et al., 2016)
5	Cr^{6+}	0.050[a]	0.100[b]	0.050[a], 0.050[b]	Kidney, liver, nervous system damage, lung cancer, bone cancer, diarrhea, and dermatitis	(Saravanan et al., 2017)
6	Ni^{2+}	---	0.05b	0.20[a], 0.02[b]	Dermatitis, allergy, respiratory system cancer	(Kinuthia et al., 2020b)

Sun *et al.* (Sun et al., 2017) reported the photocatalytic oxidation of arsenite (AsO_3^{3-}) to arsenate (AsO_4^{4-}) using CuO-Fe_3O_4 nanoparticles under visible light illumination. Ahamed *et al.* (Ahamed et al., 2020) observed about 95% removal of Ni^{2+} ions from aqueous solution using TiO_2/CuO thin film under visible light irradiation for 45 minutes. This removal performance, which was higher by 17% compared to the achievement when CuO thin film is used in the same time duration was ascribed to the better separation efficiency of photogenerated electrons and holes in the heterojunction composite which enables photoexcited electrons to react with adsorbed Ni^{2+} and reduce it to elemental Ni.

Nogueira *et al.* (Nogueira et al., 2017) reported pronounced photocatalytic reduction of Cr (VI) to Cr(III) using Nb_2O_5/CuO (10wt%) heterostructure with a removal efficiency of 78% versus 23% when a mechanical mixture of the pure oxides was employed under visible light irradiation for 210 minutes. The formation of type-II heterostructure between the two oxides results in effective charge carriers' separation due to the transfer of CB electrons from CuO to the CB of Nb_2O_5. Figure 13 (a) and higher absorption in the visible region has been proposed to be the reason for the superior removal percentage observed. In another report by Yu *et al.* (Yu et al., 2015), virtually complete reduction of Cr(VI) in aqueous solution upon irradiation under visible light for 80 minutes was found employing CuO/ZnO composite and this was higher than that achieved by the pure oxides individually under similar conditions. However, removal efficiency of only 55% was achieved during the photocatalytic reduction of the same ion specified using Cu-TiO_2/CuO photocatalyst under solar light irradiation for 4h (Nagaraju, 2020). While in a study conducted by Kadi *et al.* (Kadi et al., 2020), 100% removal of Hg^{2+} via photocatalytic reduction using 1.6 g/L of metal ion concentration and 2%CuO/g-C_3N_4 catalyst load in 30 minutes under visible light irradiation was reported.

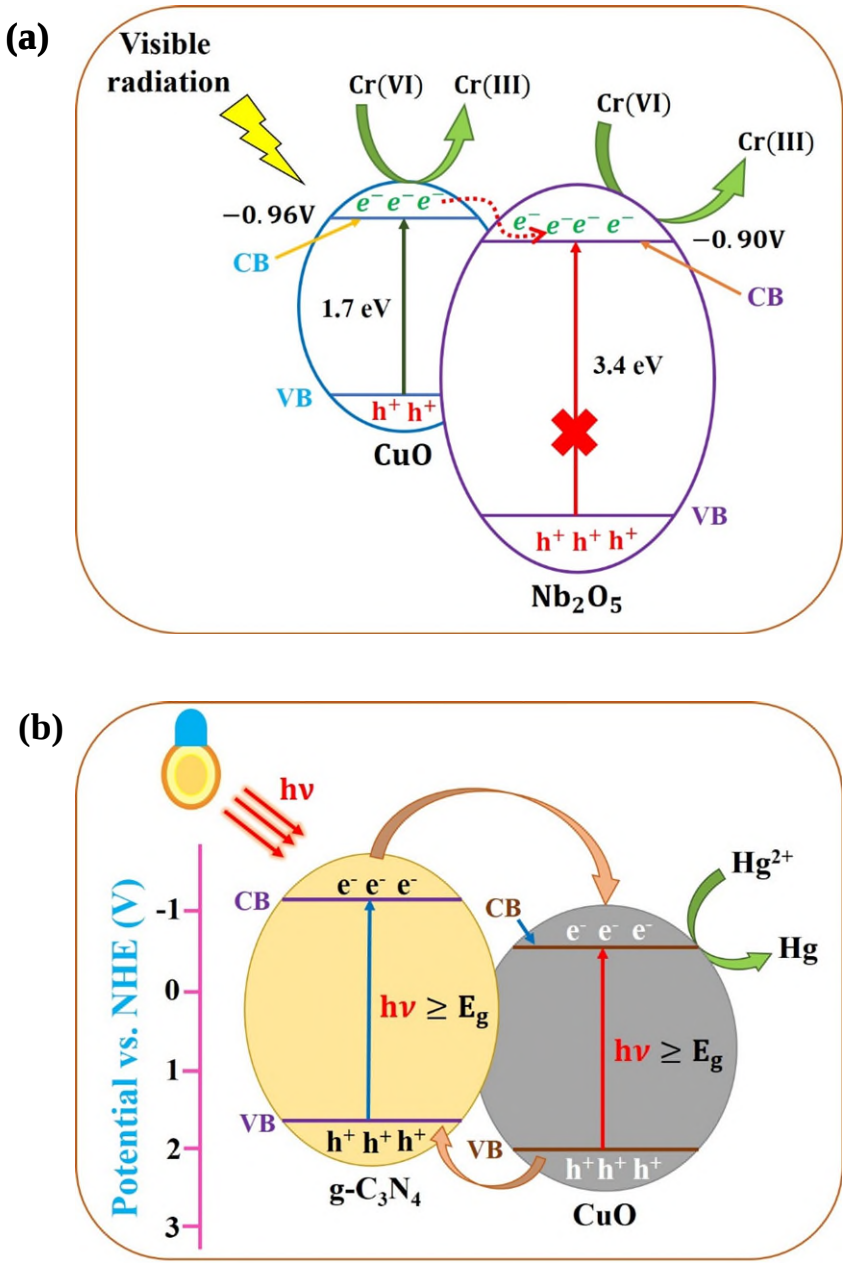

774 **Figure 13.** Removal via photocatalytic reduction of Cr (VI) using Nb_2O_5/CuO heterostructure (a)
775 (Nogueira et al., 2017) and Hg^{2+} using CuO/g-C_3N_4 mesoporous heterostructure photocatalyst (b) (Kadi et
776 al., 2020).

777 This performance achieved by the mesoporous composite catalyst was higher than that of the pure
778 phases individually and attributed the observed enhanced performance to effective e^-/h^+pairs

779 separation by the formation of heterojunction between CuO and g-C_3N_4, Figure 13 (b), dispersing
780 of small particles of CuO onto g-C_3N_4 having large surface area and small bandgap, rapid transfer
781 of the Hg^{2+} ion to the catalyst surface and also minimized light scattering owing to the mesoporous
782 structure of the catalyst. Similar higher performance photocatalytic removal of Pb^{2+} from aqueous
783 solution using graphene–CuO nanocomposites as compared to pure CuO or mechanically mixed
784 graphene and CuO nanoparticles were observed by Prashanti *et al.* (Prashanti et al., 2019a).

785 In addition, 100% removal of Hg^{2+} was achieved using 3% mesoporous CuO/ZnO
786 nanocomposite in 60 minutes under visible light irradiation which was much higher than that
787 achieved by commercial P-25 catalyst and pure ZnO nanoparticles, as reported by Mohamed *et al.*
788 (Mohamed and Ismail, 2021). The reason for the enhanced photocatalytic reduction of Hg^{2+} was
789 attributed by the researchers to be due to increased surface area and pore volume which promotes
790 mass diffusion and provides more active sites, and enhanced transfer of photogenerated charge
791 carriers as a result of the p-n heterojunction formation between p-type CuO and n-type ZnO NPs.
792 The S-type charge transfer mechanism is shown in Figure 14. The reduction reaction, in this case,
793 of Hg^{++} to Hg, occurs on the CB of the semiconductor with the more negative CB edge, while the
794 oxidation reaction occurs on the VB of the semiconductor with the more positive CB potential (Xu
795 et al., 2020).

796

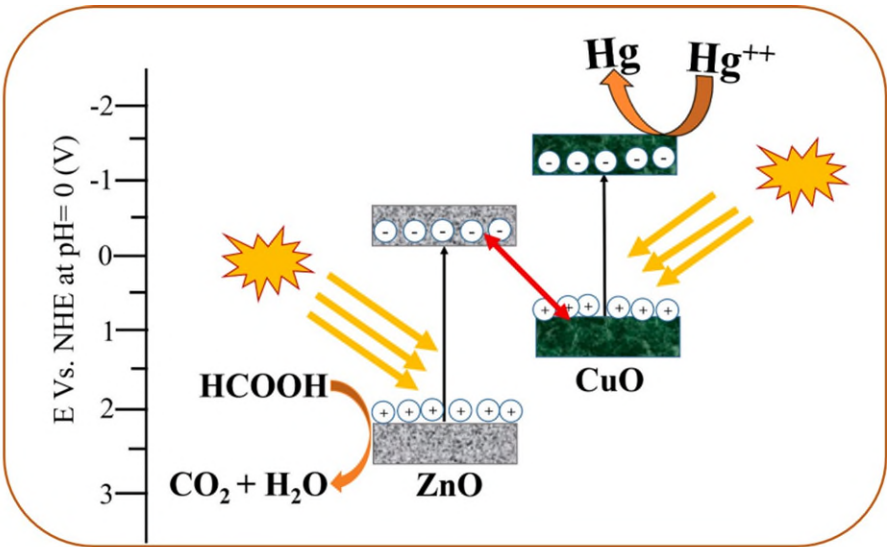

797

798 **Figure 14.** S-scheme heterojunction composite for the removal of Hg^{2+}using p-CuO/n-ZnO heterojunction
799 (Mohamed and Ismail, 2021).

800 Table 3 provides additional reports of photocatalytic removal performances achieved by CuO and
801 CuO-based catalysts for different heavy metal ions in different experimental conditions.

802 **Table 3.** Removal of toxic metal ions using CuO and CuO-based photocatalysts in different experimental
803 conditions.

S/No	Catalyst	Metal ion removed	Condition	Removal (%)	Ref.
1	CuO	Cr (VI)	Conc. of Cr(VI) = 100μM, Conc. of tartaric acid = 4μM; catalyst load = 400 mg/L, initial pH = 3 under simulated solar light irradiation for 30 min.	100	(Xu et al., 2016)
2	TiO_2/rGO/CuO	Cr (VI)	Conc. and volume of Cr (VI) = 100 ppm and 50 mL, Conc. and volume of citric acid = 0.1 ppm and1 mL; catalyst	100	(Wang et al., 2020b)

			load = 50 mg under visible light irradiation for 80 min.		
3	CuO/ZnO	As (III)	Conc. of As(III) = 30 ppm; catalyst load = 0.67 g/L under UV irradiation for 10h	100	(Samad et al., 2016)
4	Cu-TiO_2/CuO	Cr(VI)	Conc. and volume of Cr (VI) = 1mM and 100 mL; catalyst load = 10 mg under sunlight for 4h	55	(Udayabhanu et al., 2020)
5	2CuO/ZrO_2-MCM-41*	Cr(VI)	Conc. of Cr(VI) = 20 ppm; catalyst load = 1 g/L under solar light for 30 min.	99	(Nanda et al., 2017)
6	CuO	Cr (III)	Conc. and volume of Cr(III) = 200 mL of 50 ppm, 1µL of H_2O_2; catalyst load = 0.1 g, pH = 8 under 64W photoreactor for 2h	99.99	(Kondabey et al., 2019)
7	PAL†/CuO	Cr(VI)	Conc. and volume of Cr(VI) = 50 mL of 100µM, 10 mM tartaric acid; catalyst load = 0.02 g under visible light for 30min.	100	(Xu et al., 2019)
8	CuO/N-TiO_2	Hg(II)	Conc. of Hg(II) = 50 ppm; catalyst (CuO/N-TiO_2, plasma treated) load = 1 g/L at 20 ^oC under visible light for 20 min.	100	(Luo et al., 2014)

* 2CuO/ZrO_2-MCM-41 = 2Wt% of CuO in CuO/ZrO_2 supported on mesoporous material Mobil composition of Matter No. 41 (MCM-41)
† PAL = Palygorskite

9	Cu_7S_4-CuO	Ni(II)	Conc. of Ni(II) = 0.01 M; catalyst load = 4 thin films of catalysts with thickness of around 350 nm and surface area 10 cm^2 each under visible light illumination for 1h.	95	(Ghosh and Mondal, 2017)
10	Graphene-CuO	Pb(II)	Conc. and volume of Pb(II) = $5x10^{-5}$ M and 30 mL; catalyst load = 30 mg under solar light irradiation for 1h.	98	(Prashanti et al., 2019b)

804

805

806 **3. Conclusions and perspectives**

807 Copper (II) oxide is an intrinsically p-type narrow bandgap semiconductor that can generally
808 be synthesized using physical, chemical, and biological methods for multifarious applications in
809 different fields including in magnetic storage media, high-temperature superconductors, dye-
810 sensitized solar cells, fuel cells, chemical and gas sensors, as an antimicrobial agent, and the
811 heterogeneous photocatalytic removal of contaminants in wastewater treatment. Because of its
812 easy availability, low cost, narrow bandgap, excellent photochemical stability, and facile synthesis,
813 CuO has attracted attention for application in photocatalytic elimination of organic and inorganic
814 pollutants.

815 Most photodegradation reactions of organic pollutants follow pseudo-first-order reaction model
816 and *in situ* generated hydroxyl ($HO^{\cdot}$) and superoxide ion ($O_2^{-\cdot}$) radicals were primarily responsible
817 for inducing the degradation of the pollutants. The photocatalyst was at the heart of these reactions

and one that results in fast reaction kinetics and can easily be retrieved for reuse was needed for large-scale industrial application. In narrow bandgap semiconductors such as CuO, fast charge carrier recombination was a major problem that retards reactive species generation and degradation proficiency of organic pollutants. As a consequence, strategies such as elemental doping and coupling with other semiconductors or supports had been adopted to minimize the problem and augment the catalytic activity response of CuO nanostructures. This enhancement may be due to the associated improved physicochemical properties such as increased stability, raised specific surface area, and better dispersibility of the catalyst particles in aqueous media, and efficient separation of charge carriers, resulting in more reactive species generation and higher degradation. Effective charge carriers separation was achieved in optimally doped CuO nanostructures due to the dopant elements serving as traps for CB electrons, whereas, in coupled heterostructures such as type-II, separation ~~is~~ was due to diffusion of the carriers in different directions across the interface between the semiconductors after photoexcitation. One problem with type-II heterostructures was the reduction in the redox potential of the coupled semiconductors when conduction band electrons with higher CB edge potential diffuse into the other semiconductor with lower CB edge potential and VB holes in the reverse direction. However, in Z-scheme and S-scheme charge transfer mechanisms, such a problem does not exist and the redox potential of the coupled semiconductors was maintained while effectively separating the charge carriers.

In addition to charge carrier recombination, other factors that influence the rate of photodegradation of organic pollutants include morphological properties of the synthesized CuO and CuO-based nanostructure, type of organic pollutant, and operational parameters such as catalyst dose and pollutant initial concentration, pH, temperature, aeration and stirring rate, energy

and intensity of radiation utilized, and the presence of oxidants and other interferents in the reaction mixture.

Photocatalysis is also a promising technique for removing toxic metal ions from aqueous media. Since heavy metal ions are recalcitrant to bio and photodegradation, their oxidation state changed instead during the process. The objective is to change their oxidation state to a less toxic elemental or ionic state, for example, Cr(VI) to Cr(III), Hg(II) to Hg, etc. Like in the case of organic pollutants, photocatalytic removal of toxic metal ions is advantageous due to eco-friendly, low cost which involves the elimination of the ions, and is also a viable option for retrieving precious metals such as silver, gold, and platinum from wastewater.

Even though heterogeneous photocatalysis is comparatively cost-effective, easier to operate, and an environmentally friendly technique of eliminating organic and inorganic pollutants, it has its limitations that should be overcome to ensure effective removal proficiency on a large scale and be used in practical real wastewater treatments. The prominent ones include a lack of complete understanding of the reaction mechanism owing to the complex nature of the reaction, with several factors which simultaneously could affect the degree of pollutant elimination, and the challenge of obtaining a single catalyst synthesized easily in a green manner. Moreover, as the objective is to treat water-bearing toxic contaminants and get desired quality water, it is important to consider integrating photocatalysis with other treatment approaches such as adsorption to supplement its removal efficiency, especially, in cases where photocatalysis is not as such effective or becomes technically inconvenient.

Conflict of interest

The authors declare no potential conflict of interest regarding the publication of this work.

Acknowledgments

The authors would like to acknowledge the financial support provided by a Research University grant from the University of Malaya (RU003-2021). The authors acknowledge support from the ERC Synergy Grant Surface-Confined fast modulated Plasma for process and Energy intensification (SCOPE) from the European Commission with Grant No. 810182.

References

Abdullah, A.H., Peng, W.T., Hussein, M., 2016. Degradation of methylene blue dye by CuO-$BiVO_4$ photocatalysts under visible light irradiation. Malaysian Journal of Analytical Sciences 20, 1338-1345.

Ahamad, T., Naushad, M., Al-Saeedi, S.I., Almotairi, S., Alshehri, S.M., 2020a. Fabrication of MoS_2/ZnS embedded in N/S doped carbon for the photocatalytic degradation of pesticide. Materials Letters 263, 127271.

Ahamad, T., Naushad, M., Al-Shahrani, T., Al-hokbany, N., Alshehri, S.M., 2020b. Preparation of chitosan based magnetic nanocomposite for tetracycline adsorption: Kinetic and thermodynamic studies. International Journal of Biological Macromolecules 147, 258-267.

Ahamad, T., Naushad, M., Ruksana, Alhabarah, A.N., Alshehri, S.M., 2019. N/S doped highly porous magnetic carbon aerogel derived from sugarcane bagasse cellulose for the removal of bisphenol-A. International Journal of Biological Macromolecules 132, 1031-1038.

Ahamed, S.T., Ghosh, A., Show, B., Mondal, A., 2020. Fabrication of n-TiO_2/p-CuO thin-film heterojunction for efficient photocatalytic degradation of toxic organic dyes and reduction of metal ions in solution. Journal of Materials Science: Materials in Electronics 31, 16616-16633.

Ahmad, S.Z.N., Wan Salleh, W.N., Ismail, A.F., Yusof, N., Mohd Yusop, M.Z., Aziz, F., 2020. Adsorptive removal of heavy metal ions using graphene-based nanomaterials: Toxicity, roles of functional groups and mechanisms. Chemosphere 248, 126008.

Ajmal, A., Majeed, I., Malik, R.N., Idriss, H., Nadeem, M.A., 2014. Principles and mechanisms of photocatalytic dye degradation on TiO_2 based photocatalysts: a comparative overview. Rsc Advances 4, 37003-37026.

Akintelu, S.A., Folorunso, A.S., Folorunso, F.A., Oyebamiji, A.K., 2020. Green synthesis of copper oxide nanoparticles for biomedical application and environmental remediation. Heliyon 6, e04508-e04508.

Akram, N., Guo, J., Ma, W., Guo, Y., Hassan, A., Wang, J., 2020. Synergistic catalysis of $Co(OH)_2$/CuO for the Degradation of organic pollutant Under Visible Light irradiation. Scientific reports 10, 1-12.

Al-Kahtani, A.A., Alshehri, S.M., Naushad, M., Ruksana, Ahamad, T., 2019. Fabrication of highly porous N/S doped carbon embedded with ZnS as highly efficient photocatalyst for degradation of bisphenol. International Journal of Biological Macromolecules 121, 415-423.

Alp, E., Eşgin, H., Kazmanlı, M.K., Genc, A., 2019. Synergetic activity enhancement in 2D CuO-Fe_2O_3 nanocomposites for the photodegradation of rhodamine B. Ceramics International 45, 9174-9178.

Aminuzzaman, M., Kei, L.M., Liang, W.H., 2017. Green synthesis of copper oxide (CuO) nanoparticles using banana peel extract and their photocatalytic activities. AIP Conference Proceedings 1828, 020016.

Arunadevi, R., Kavitha, B., Rajarajan, M., Suganthi, A., Jeyamurugan, A., 2018. Investigation of the drastic improvement of photocatalytic degradation of Congo red by monoclinic Cd, Ba-CuO nanoparticles and its antimicrobial activities. Surfaces and Interfaces 10, 32-44.

Bai, W., Wu, M., Du, X., Gong, W., Ding, Y., Song, C., Liu, L., 2021. Synergistic effect of multiple-phase rGO/CuO/Cu_2O heterostructures for boosting photocatalytic activity and durability. Applied Surface Science 544, 148607.

Bajiri, M.A., Hezam, A., Namratha, K., Viswanath, R., Drmosh, Q., Naik, H.B., Byrappa, K., 2019. CuO/ZnO/g-C_3N_4 heterostructures as efficient visible light-driven photocatalysts. Journal of Environmental Chemical Engineering 7, 103412.

Benabbas, K., Zabat, N., Hocini, I., 2021. Facile synthesis of Fe_3O_4/CuO a core-shell heterostructure for the enhancement of photocatalytic activity under visible light irradiation. Environmental Science and Pollution Research 28, 4329-4341.

Bhattacharjee, A., Ahmaruzzaman, M., 2016. CuO nanostructures: facile synthesis and applications for enhanced photodegradation of organic compounds and reduction of p-nitrophenol from aqueous phase. RSC Advances 6, 41348-41363.

Botsa, S.M., Basavaiah, K., 2018. Removal of Nitrophenols from wastewater by monoclinic CuO/RGO nanocomposite. Nanotechnology for Environmental Engineering 4, 1.

Chauhan, M., Kaur, N., Bansal, P., Kumar, R., Srinivasan, S., Chaudhary, G.R., 2020. Proficient Photocatalytic and Sonocatalytic Degradation of Organic Pollutants Using CuO Nanoparticles. Journal of Nanomaterials 2020, 6123178.

Chen, R.X., Zhu, S.L., Mao, J., Cui, Z.D., Yang, X.J., Liang, Y.Q., Li, Z.Y., 2015. Synthesis of CuO/Co_3O_4 Coaxial Heterostructures for Efficient and Recycling Photodegradation. International Journal of Photoenergy 2015, 183468.

Contreras Rodríguez, A.R., 2015. Removal of cadmium (II), lead (II) and chromium (VI) in water with nanomaterials. Universitat Autònoma de Barcelona.

Crini, G., Lichtfouse, E., 2019. Advantages and disadvantages of techniques used for wastewater treatment. Environmental Chemistry Letters 17, 145-155.

Cui, Y., Tang, Y., Wang, X., 2015. Template-free synthesis of graphitic carbon nitride hollow spheres for photocatalytic degradation of organic pollutants. Materials Letters 161, 197-200.

Dasineh Khiavi, N., Katal, R., Kholghi Eshkalak, S., Masudy-Panah, S., Ramakrishna, S., Jiangyong, H., 2019. Visible Light Driven Heterojunction Photocatalyst of CuO–Cu2O Thin Films for Photocatalytic Degradation of Organic Pollutants. Nanomaterials 9, 1011.

Date, M.K., Yang, L.-H., Yang, T.-Y., Wang, K.-y., Su, T.-Y., Wu, D.-C., Cheuh, Y.-L., 2020. Three-dimensional CuO/TiO_2 hybrid nanorod arrays prepared by electrodeposition in AAO membranes as an excellent Fenton-like photocatalyst for dye degradation. Nanoscale research letters 15, 1-12.

Dhineshbabu, N.R., Rajendran, V., Nithyavathy, N., Vetumperumal, R., 2016. Study of structural and optical properties of cupric oxide nanoparticles. Applied Nanoscience 6, 933-939.

Dursun, S., Koyuncu, S.N., Kaya, İ.C., Kaya, G.G., Kalem, V., Akyildiz, H., 2020. Production of $CuO–WO_3$ hybrids and their dye removal capacity/performance from wastewater by adsorption/photocatalysis. Journal of Water Process Engineering 36, 101390.

Dutta, S., Das, K., Chakrabarti, K., Jana, D., De, S., De, S., 2016. Highly efficient photocatalytic activity of CuO quantum dot decorated rGO nanocomposites. Journal of Physics D: Applied Physics 49, 315107.

El Sayed, A.M., Shaban, M., 2015. Structural, optical and photocatalytic properties of Fe and (Co, Fe) co-doped copper oxide spin coated films. Spectrochimica Acta Part A: Molecular and Biomolecular Spectroscopy 149, 638-646.

Fahmi Khairol, N., Sapawe, N., Danish, M., 2019. Excellent Performance Integrated Both Adsorption and Photocatalytic Reaction Toward Degradation of Congo Red by CuO/Eggshell. Materials Today: Proceedings 19, 1340-1345.

Fang, M., Tan, X., Liu, Z., Hu, B., Wang, X., 2021. Recent progress on metal-enhanced photocatalysis: a review on the mechanism. Research 2021, 1-16.

Garrido-Cardenas, J.A., Esteban-García, B., Agüera, A., Sánchez-Pérez, J.A., Manzano-Agugliaro, F., 2020. Wastewater Treatment by Advanced Oxidation Process and Their Worldwide Research Trends. International Journal of Environmental Research and Public Health 17, 170.

Ghosh, A., Mondal, A., 2017. Efficient charge separation in mixed phase Cu_7S_4-CuO thin film: Enhanced photocatalytic reduction of aqueous Ni (II) under visible-light. Thin Solid Films 628, 68-74.

Hao, M., Qiu, M., Yang, H., Hu, B., Wang, X., 2021. Recent advances on preparation and environmental applications of MOF-derived carbons in catalysis. Science of The Total Environment 760, 143333.

Haseena, S., Shanavas, S., Duraimurugan, J., Ahamad, T., Alshehri, S.M., Acevedo, R., Jayamani, N., 2019. Investigation on photocatalytic and antibacterial ability of green treated copper oxide nanoparticles using Artabotrys Hexapetalus and Bambusa Vulgaris plant extract. Materials Research Express 6, 125064.

Hasija, V., Kumar, A., Sudhaik, A., Raizada, P., Singh, P., Van Le, Q., Le, T.T., Nguyen, V.-H., 2021a. Step-scheme heterojunction photocatalysts for solar energy, water splitting, CO_2 conversion, and bacterial inactivation: a review. Environmental Chemistry Letters 19, 2941-2966.

Hasija, V., Nguyen, V.-H., Kumar, A., Raizada, P., Krishnan, V., Khan, A.A.P., Singh, P., Lichtfouse, E., Wang, C., Thi Huong, P., 2021b. Advanced activation of persulfate by polymeric g-C_3N_4 based photocatalysts for environmental remediation: A review. Journal of Hazardous Materials 413, 125324.

Hasija, V., Patial, S., Raizada, P., Aslam Parwaz Khan, A., Asiri, A.M., Van Le, Q., Nguyen, V.-H., Singh, P., 2022. Covalent organic frameworks promoted single metal atom catalysis: Strategies and applications. Coordination Chemistry Reviews 452, 214298.

Hossain, S.S., Tarek, M., Munusamy, T.D., Karim, K.M.R., Roopan, S.M., Sarkar, S.M., Cheng, C.K., Khan, M.M.R., 2020. Facile synthesis of CuO/CdS heterostructure photocatalyst for the effective degradation of dye under visible light. Environmental Research 188, 109803.

Ighalo, J.O., Sagboye, P.A., Umenweke, G., Ajala, O.J., Omoarukhe, F.O., Adeyanju, C.A., Ogunniyi, S., Adeniyi, A.G., 2021. CuO nanoparticles (CuO NPs) for water treatment: A review of recent advances. Environmental Nanotechnology, Monitoring & Management 15, 100443.

Imtiaz, F., Rashid, J., Xu, M., 2019. Semiconductor Nanocomposites for Visible Light Photocatalysis of Water Pollutants. Concepts of Semiconductor Photocatalysis. IntechOpen.

Iqbal, S., Javed, M., Bahadur, A., Qamar, M.A., Ahmad, M., Shoaib, M., Raheel, M., Ahmad, N., Akbar, M.B., Li, H., 2020. Controlled synthesis of Ag-doped CuO nanoparticles as a core with poly (acrylic acid) microgel shell for efficient removal of methylene blue under visible light. Journal of Materials Science: Materials in Electronics 31, 8423-8435.

993 Joseph, C.G., Li Puma, G., Bono, A., Krishnaiah, D., 2009. Sonophotocatalysis in advanced
994 oxidation process: A short review. Ultrasonics Sonochemistry 16, 583-589.
995 Junior, O.S., Monteiro, A., Oliveira, J., Araújo, A., Silva, D., Kulesza, J., Barros, B., 2019.
996 Coordination polymer-derived CuO catalysts for oxidative degradation of methylene blue.
997 Materials Chemistry and Physics 235, 121737.
998 Kadi, M.W., Mohamed, R.M., Ismail, A.A., Bahnemann, D.W., 2020. Soft and hard templates
999 assisted synthesis mesoporous CuO/g-C_3N_4 heterostructures for highly enhanced and accelerated
1000 Hg(II) photoreduction under visible light. Journal of Colloid and Interface Science 580, 223-233.
1001 Karthikeyan, S., Chuaicham, C., Pawar, R.R., Sasaki, K., Li, W., Lee, A.F., Wilson, K., 2019.
1002 Template free mild hydrothermal synthesis of core–shell Cu_2O(Cu)@CuO visible light
1003 photocatalysts for N-acetyl-para-aminophenol degradation. Journal of Materials Chemistry A 7,
1004 20767-20777.
1005 Katal, R., Masudy-Panah, S., Sabbaghan, M., Hossaini, Z., Davood Abadi Farahani, M.H., 2020.
1006 Photocatalytic degradation of triclosan by oxygen defected CuO thin film. Separation and
1007 Purification Technology 250, 117239.
1008 Katwal, R., Kaur, H., Sharma, G., Naushad, M., Pathania, D., 2015. Electrochemical synthesized
1009 copper oxide nanoparticles for enhanced photocatalytic and antimicrobial activity. Journal of
1010 Industrial and Engineering Chemistry 31, 173-184.
1011 Khatri, N., Tyagi, S., 2015. Influences of natural and anthropogenic factors on surface and
1012 groundwater quality in rural and urban areas. Frontiers in Life Science 8, 23-39.
1013 Kinuthia, G.K., Ngure, V., Beti, D., Lugalia, R., Wangila, A., Kamau, L., 2020a. Levels of heavy
1014 metals in wastewater and soil samples from open drainage channels in Nairobi, Kenya:
1015 community health implication. Scientific Reports 10, 8434.

Kinuthia, G.K., Ngure, V., Beti, D., Lugalia, R., Wangila, A., Kamau, L., 2020b. Levels of heavy metals in wastewater and soil samples from open drainage channels in Nairobi, Kenya: Community health implication. Scientific Reports 10, 1-13.

Kodavanti, P.R.S., Royland, J.E., Sambasiva Rao, K.R.S., 2014. Toxicology of Persistent Organic Pollutants. Reference Module in Biomedical Sciences. Elsevier.

Koe, W.S., Lee, J.W., Chong, W.C., Pang, Y.L., Sim, L.C., 2020. An overview of photocatalytic degradation: photocatalysts, mechanisms, and development of photocatalytic membrane. Environmental Science and Pollution Research 27, 2522-2565.

Kondabey, J., Ghorbani, M.H., Aghaie, H., Fazaeli, R., 2019. Study of the adsorption and photocatalytic properties of copper oxide with different morphologies in removal of Cr(III) ion from aqueous media. Water Science and Technology 80, 827-835.

Koohestani, H., 2019. Photocatalytic performance of rod-shaped copper oxides prepared by spin coating. Micro & Nano Letters 14, 339-343.

Kumar, A., Raizada, P., Hosseini-Bandegharaei, A., Thakur, V.K., Nguyen, V.-H., Singh, P., 2021. C-, N-Vacancy defect engineered polymeric carbon nitride towards photocatalysis: viewpoints and challenges. Journal of Materials Chemistry A 9, 111-153.

Kumaresan, N., Sinthiya, M.M.A., Ramamurthi, K., Ramesh Babu, R., Sethuraman, K., 2020. Visible light driven photocatalytic activity of ZnO/CuO nanocomposites coupled with rGO heterostructures synthesized by solid-state method for RhB dye degradation. Arabian Journal of Chemistry 13, 3910-3928.

Le, A.T., Pung, S.-Y., Sreekantan, S., Matsuda, A., Huynh, D.P., 2019a. Mechanisms of removal of heavy metal ions by ZnO particles. Heliyon 5, e01440.

Le, A.T., Pung, S.-Y., Sreekantan, S., Matsuda, A., Huynh, D.P., 2019b. Mechanisms of removal of heavy metal ions by ZnO particles. Heliyon 5, e01440-e01440.

Li, W., He, S.-a., Su, Z.-y., Xu, W., Wang, X.-c., 2019. A BiOCl-CuO photocatalyst based on p-n heterojunction and its photocatalytic performance under visible-light. Applied Surface Science 470, 707-715.

Li, Y., Chen, C., Wu, Y., Han, Y., Lan, Y., 2017. Assessing the Photocatalytic Reduction of Cr(VI) by CuO in Combination with Different Organic Acids. Water, Air, & Soil Pollution 228, 363.

Liu, S., Tian, J., Wang, L., Luo, Y., Sun, X., 2012. One-pot synthesis of CuO nanoflower-decorated reduced graphene oxide and its application to photocatalytic degradation of dyes. Catalysis Science & Technology 2, 339-344.

Liu, X., Ma, R., Zhuang, L., Hu, B., Chen, J., Liu, X., Wang, X., 2021. Recent developments of doped g-C_3N_4 photocatalysts for the degradation of organic pollutants. Critical Reviews in Environmental Science and Technology 51, 751-790.

Luo, Z., Jiang, H., Hu, L., Li, D., Geng, W., Wei, P., 2014. Effect of N_2/Ar plasma treatment on the visible light photocatalytic activity of CuO/TiO_2. Chinese Journal of Catalysis 35, 1752-1760.

Mageshwari, K., Nataraj, D., Pal, T., Sathyamoorthy, R., Park, J., 2015. Improved photocatalytic activity of ZnO coupled CuO nanocomposites synthesized by reflux condensation method. Journal of Alloys and Compounds 625, 362-370.

Mahmud, H.N.M.E., Huq, A.K.O., Yahya, R.b., 2016. The removal of heavy metal ions from wastewater/aqueous solution using polypyrrole-based adsorbents: a review. RSC Advances 6, 14778-14791.

Mallick, P., Sahu, S., 2012. Structure, microstructure and optical absorption analysis of CuO nanoparticles synthesized by sol-gel route. Nanoscience and Nanotechnology 2, 71-74.

Mohamed, R.M., Ismail, A.A., 2021. Photocatalytic reduction and removal of mercury ions over mesoporous CuO/ZnO S-scheme heterojunction photocatalyst. Ceramics International 47, 9659-9667.

Mrunal, V.K., Vishnu, A.K., Momin, N., Manjanna, J., 2019. Cu_2O nanoparticles for adsorption and photocatalytic degradation of methylene blue dye from aqueous medium. Environmental Nanotechnology, Monitoring & Management 12, 100265.

Muhd Julkapli, N., Bagheri, S., Bee Abd Hamid, S., 2014. Recent Advances in Heterogeneous Photocatalytic Decolorization of Synthetic Dyes. The Scientific World Journal 2014, 692307.

Mukwevho, N., Fosso-Kankeu, E., Waanders, F., Kumar, N., Ray, S.S., Mbianda, X.Y., 2019. Photocatalytic activity of $Gd_2O_2CO_3$ ZnO CuO nanocomposite used for the degradation of phenanthrene. SN Applied Sciences 1, 1-11.

Munawar, T., Mukhtar, F., Yasmeen, S., Naveed-ur-Rehman, M., Nadeem, M.S., Riaz, M., Mansoor, M., Iqbal, F., 2021. Sunlight-induced photocatalytic degradation of various dyes and bacterial inactivation using CuO–MgO–ZnO nanocomposite. Environmental Science and Pollution Research 28, 42243-42260.

Murali, D.S., Aryasomayajula, S., 2018. Thermal conversion of Cu_4O_3 into CuO and Cu_2O and the electrical properties of magnetron sputtered Cu_4O_3 thin films. Applied Physics A 124, 279.

Muthuvel, A., Jothibas, M., Manoharan, C., 2020. Synthesis of copper oxide nanoparticles by chemical and biogenic methods: photocatalytic degradation and in vitro antioxidant activity. Nanotechnology for Environmental Engineering 5, 1-19.

Nagaraju, G., 2020. One-pot synthesis of Cu-TiO_2/CuO nanocomposite: Application to photocatalysis for enhanced H2 production, dye degradation & detoxification of Cr (VI). international journal of hydrogen energy 45, e7828.

Nanda, B., Pradhan, A.C., Parida, K.M., 2017. Fabrication of mesoporous CuO/ZrO_2-MCM-41 nanocomposites for photocatalytic reduction of Cr(VI). Chemical Engineering Journal 316, 1122-1135.

Nazim, M., Khan, A.A.P., Asiri, A.M., Kim, J.H., 2021. Exploring Rapid Photocatalytic Degradation of Organic Pollutants with Porous CuO Nanosheets: Synthesis, Dye Removal, and Kinetic Studies at Room Temperature. ACS Omega 6, 2601-2612.

Neena, D., Kondamareddy, K.K., Bin, H., Lu, D., Kumar, P., Dwivedi, R.K., Pelenovich, V.O., Zhao, X.-Z., Gao, W., Fu, D., 2018. Enhanced visible light photodegradation activity of RhB/MB from aqueous solution using nanosized novel Fe-Cd co-modified ZnO. Scientific Reports 8, 10691.

Nogueira, A.E., Lopes, O.F., Neto, A.B.S., Ribeiro, C., 2017. Enhanced Cr(VI) photoreduction in aqueous solution using Nb_2O_5/CuO heterostructures under UV and visible irradiation. Chemical Engineering Journal 312, 220-227.

Norzaee, S., Djahed, B., Khaksefidi, R., Mostafapour, F.K., 2017. Photocatalytic degradation of aniline in water using CuO nanoparticles. Journal of Water Supply: Research and Technology-Aqua 66, 178-185.

Nuengmatcha, P., Porrawatkul, P., Chanthai, S., Sricharoen, P., Limchoowong, N., 2019. Enhanced photocatalytic degradation of methylene blue using Fe_2O_3/graphene/CuO nanocomposites under visible light. Journal of Environmental Chemical Engineering 7, 103438.

Pakzad, K., Alinezhad, H., Nasrollahzadeh, M., 2020. Euphorbia polygonifolia extract assisted biosynthesis of Fe_3O_4@CuO nanoparticles: Applications in the removal of metronidazole, ciprofloxacin and cephalexin antibiotics from aqueous solutions under UV irradiation. Applied Organometallic Chemistry 34, e5910.

Pareek, A., Venkata Mohan, S., 2019. Chapter 1.4 - Graphene and Its Applications in Microbial Electrochemical Technology. in: Mohan, S.V., Varjani, S., Pandey, A. (Eds.). Microbial Electrochemical Technology. Elsevier, pp. 75-97.

Patial, S., Raizada, P., Hasija, V., Singh, P., Thakur, V.K., Nguyen, V.H., 2021. Recent advances in photocatalytic multivariate metal organic frameworks-based nanostructures toward renewable energy and the removal of environmental pollutants. Materials Today Energy 19, 100589.

Phang, Y.-K., Aminuzzaman, M., Akhtaruzzaman, M., Muhammad, G., Ogawa, S., Watanabe, A., Tey, L.-H., 2021. Green Synthesis and Characterization of CuO Nanoparticles Derived from Papaya Peel Extract for the Photocatalytic Degradation of Palm Oil Mill Effluent (POME). Sustainability 13, 796.

Pirilä, M., Saouabe, M., Ojala, S., Rathnayake, B., Drault, F., Valtanen, A., Huuhtanen, M., Brahmi, R., Keiski, R.L., 2015. Photocatalytic degradation of organic pollutants in wastewater. Topics in Catalysis 58, 1085-1099.

Prashanti, B., Sreevani, I., Suresh, B., Damodharam, T., 2019a. Graphene-CuO nanocomposite for Efficient Photocatalytic Reduction of Pb (II) under Solar Light Irradiation. Applied Ecology and Environmental Sciences 7, 176-181.

Prashanti, B., Sreevani, I., Suresh, B., Damodharam, T., 2019b. Graphene-CuO nanocomposite for Efficient Photocatalytic Reduction of Pb(II) under Solar Light Irradiation. Applied Ecology and Environmental Sciences 7, 176-181.

Priya, R., Stanly, S., Dhanalekshmi, S.B., Sagadevan, S., 2019. Fabrication of photocatalyst MgO: CuO composite and enhancement of photocatalytic activity under UV light. Materials Research Express 6, 125023.

Qiu, M., Hu, B., Chen, Z., Yang, H., Zhuang, L., Wang, X., 2021a. Challenges of organic pollutant photocatalysis by biochar-based catalysts. Biochar 3, 117-123.

Qiu, M., Liu, Z., Wang, S., Hu, B., 2021b. The photocatalytic reduction of U(VI) into U(IV) by ZIF-8/g-C_3N_4 composites at visible light. Environmental Research 196, 110349.

Raha, S., Mohanta, D., Ahmaruzzaman, M., 2021. Novel CuO/Mn_3O_4/ZnO nanocomposite with superior photocatalytic activity for removal of Rabeprazole from water. Scientific Reports 11, 15187.

Raizada, P., Sudhaik, A., Patial, S., Hasija, V., Parwaz Khan, A.A., Singh, P., Gautam, S., Kaur, M., Nguyen, V.-H., 2020. Engineering nanostructures of CuO-based photocatalysts for water treatment: Current progress and future challenges. Arabian Journal of Chemistry 13, 8424-8457.

Rajamanickam, D., Shanthi, M., 2016. Photocatalytic degradation of an organic pollutant by zinc oxide–solar process. Arabian Journal of Chemistry 9, S1858-S1868.

Rao, M.P., Wu, J.J., Asiri, A.M., Anandan, S., 2017. Photocatalytic degradation of tartrazine dye using CuO straw-sheaf-like nanostructures. Water Science and Technology 75, 1421-1430.

Ren, G., Han, H., Wang, Y., Liu, S., Zhao, J., Meng, X., Li, Z., 2021. Recent Advances of Photocatalytic Application in Water Treatment: A Review. Nanomaterials 11, 1804.

Revellame, E.D., Fortela, D.L., Sharp, W., Hernandez, R., Zappi, M.E., 2020. Adsorption kinetic modeling using pseudo-first order and pseudo-second order rate laws: A review. Cleaner Engineering and Technology 1, 100032.

Sadollahkhani, A., Hussain Ibupoto, Z., Elhag, S., Nur, O., Willander, M., 2014. Photocatalytic properties of different morphologies of CuO for the degradation of Congo red organic dye. Ceramics International 40, 11311-11317.

Sagadevan, S., Lett, J.A., Weldegebrieal, G.K., Garg, S., Oh, W.-C., Hamizi, N.A., Johan, M.R., 2021. Enhanced Photocatalytic Activity of rGO-CuO Nanocomposites for the Degradation of Organic Pollutants. Catalysts 11, 1008.

Sakib, A.A.M., Masum, S.M., Hoinkis, J., Islam, R., Molla, M.A.I., 2019. Synthesis of CuO/ZnO Nanocomposites and Their Application in Photodegradation of Toxic Textile Dye. Journal of Composites Science 3, 91.

Samad, A., Furukawa, M., Katsumata, H., Suzuki, T., Kaneco, S., 2016. Photocatalytic oxidation and simultaneous removal of arsenite with CuO/ZnO photocatalyst. Journal of Photochemistry and Photobiology A: Chemistry 325, 97-103.

Sapkota, K.P., Lee, I., Hanif, M., Islam, M., Akter, J., Hahn, J.R., 2020. Enhanced visible-light photocatalysis of nanocomposites of copper oxide and single-walled carbon nanotubes for the degradation of methylene blue. Catalysts 10, 297.

Saravanan, A., Kumar, P.S., Yashwanthraj, M., 2017. Sequestration of toxic Cr (VI) ions from industrial wastewater using waste biomass: A review. Desalination and Water Treatment 68, 245-266.

Saravanan, R., Karthikeyan, S., Gupta, V., Sekaran, G., Narayanan, V., Stephen, A., 2013. Enhanced photocatalytic activity of ZnO/CuO nanocomposite for the degradation of textile dye on visible light illumination. Materials Science and Engineering: C 33, 91-98.

Sasikala, R., Karthikeyan, K., Easwaramoorthy, D., Bilal, I.M., Rani, S.K., 2016. Photocatalytic degradation of trypan blue and methyl orange azo dyes by cerium loaded CuO nanoparticles. Environmental Nanotechnology, Monitoring & Management 6, 45-53.

Sharma, A., Dutta, R.K., Roychowdhury, A., Das, D., 2016. Studies on structural defects in bare, PVP capped and TPPO capped copper oxide nanoparticles by positron annihilation lifetime spectroscopy and their impact on photocatalytic degradation of rhodamine B. RSC Advances 6, 74812-74821.

Sharma, K., Dutta, V., Sharma, S., Raizada, P., Hosseini-Bandegharaei, A., Thakur, P., Singh, P., 2019. Recent advances in enhanced photocatalytic activity of bismuth oxyhalides for efficient photocatalysis of organic pollutants in water: A review. Journal of Industrial and Engineering Chemistry 78, 1-20.

Sharma, S., Dutta, V., Raizada, P., Hosseini-Bandegharaei, A., Singh, P., Nguyen, V.-H., 2021. Tailoring cadmium sulfide-based photocatalytic nanomaterials for water decontamination: a review. Environmental Chemistry Letters 19, 271-306.

Sharma, V.K., Sohn, M., 2009. Aquatic arsenic: Toxicity, speciation, transformations, and remediation. Environment International 35, 743-759.

Shrestha, R., Ban, S., Devkota, S., Sharma, S., Joshi, R., Tiwari, A.P., Kim, H.Y., Joshi, M.K., 2021. Technological trends in heavy metals removal from industrial wastewater: A review. Journal of Environmental Chemical Engineering 9, 105688.

Sibhatu, A.K., Weldegebrieal, G.K., Imteyaz, S., Sagadevan, S., Tran, N.N., Hessel, V., 2022. Synthesis and process parametric effects on the photocatalyst efficiency of CuO nanostructures for decontamination of toxic heavy metal ions. Chemical Engineering and Processing - Process Intensification 173, 108814.

Singh, G., Panday, S., Rawat, M., Kukkar, D., Basu, S., 2017. Facile synthesis of CuO semiconductor nanorods for time dependent study of dye degradation and bioremediation applications. Journal of Nano Research. Trans Tech Publ, pp. 154-164.

Singh, J., Kumar, V., Kim, K.-H., Rawat, M., 2019. Biogenic synthesis of copper oxide nanoparticles using plant extract and its prodigious potential for photocatalytic degradation of dyes. Environmental Research 177, 108569.

Sonia, S., Annsi, I.J., Kumar, P.S., Mangalaraj, D., Viswanathan, C., Ponpandian, N., 2015a. Hydrothermal synthesis of novel Zn doped CuO nanoflowers as an efficient photodegradation material for textile dyes. Materials Letters 144, 127-130.

Sonia, S., Jose Annsi, I., Suresh Kumar, P., Mangalaraj, D., Viswanathan, C., Ponpandian, N., 2015b. Hydrothermal synthesis of novel Zn doped CuO nanoflowers as an efficient photodegradation material for textile dyes. Materials Letters 144, 127-130.

Sonu, Dutta, V., Sharma, S., Raizada, P., Hosseini-Bandegharaei, A., Kumar Gupta, V., Singh, P., 2019. Review on augmentation in photocatalytic activity of $CoFe_2O_4$ via heterojunction formation for photocatalysis of organic pollutants in water. Journal of Saudi Chemical Society 23, 1119-1136.

Srivastav, A.L., Ranjan, M., 2020. Chapter 1 - Inorganic water pollutants. in: Devi, P., Singh, P., Kansal, S.K. (Eds.). Inorganic Pollutants in Water. Elsevier, pp. 1-15.

Sun, T., Zhao, Z., Liang, Z., Liu, J., Shi, W., Cui, F., 2017. Efficient As(III) removal by magnetic CuO-Fe_3O_4 nanoparticles through photo-oxidation and adsorption under light irradiation. Journal of Colloid and Interface Science 495, 168-177.

Tadjarodi, A., Akhavan, O., Bijanzad, K., 2015. Photocatalytic activity of CuO nanoparticles incorporated in mesoporous structure prepared from bis(2-aminonicotinato) copper(II) microflakes. Transactions of Nonferrous Metals Society of China 25, 3634-3642.

Tiginyanu, I.M., Lupan, O., Ursaki, V.V., Chow, L., Enachi, M., 2011. 3.11 - Nanostructures of Metal Oxides. in: Bhattacharya, P., Fornari, R., Kamimura, H. (Eds.). Comprehensive Semiconductor Science and Technology. Elsevier, Amsterdam, pp. 396-479.

Tran, T.K., Leu, H.J., Chiu, K.F., Lin, C.Y., 2017. Electrochemical Treatment of Heavy Metal-containing Wastewater with the Removal of COD and Heavy Metal Ions. Journal of the Chinese Chemical Society 64, 493-502.

Tzvetkov, G., Zaharieva, J., Tsvetkov, M., Spassov, T., 2019. A novel construction of Z-scheme CuO/g-C_3N_4 heterojunction for visible-light-driven photocatalysis in natural seawater. International Conference on Quantum, Nonlinear, and Nanophotonics 2019 (ICQNN 2019). International Society for Optics and Photonics, p. 113320B.

Udayabhanu, Lakshmana Reddy, N., Shankar, M.V., Sharma, S.C., Nagaraju, G., 2020. One-pot synthesis of Cu–TiO_2/CuO nanocomposite: Application to photocatalysis for enhanced H_2 production, dye degradation & detoxification of Cr (VI). International Journal of Hydrogen Energy 45, 7813-7828.

Umar, M., Aziz, H.A., 2013. Photocatalytic degradation of organic pollutants in water. Organic pollutants-monitoring, risk and treatment 8, 196-197.

Vaidehi, D., Bhuvaneshwari, V., Bharathi, D., Sheetal, B.P., 2018. Antibacterial and photocatalytic activity of copper oxide nanoparticles synthesized using Solanum lycopersicum leaf extract. Materials Research Express 5, 085403.

Venkata, A.L.K., Anthony, S.P., Muthuraman, M.S., 2019. Synthesis of Solanum nigrum mediated copper oxide nanoparticles and their photocatalytic dye degradation studies. Materials Research Express 6, 125402.

Verma, N., Kumar, N., 2019. Synthesis and Biomedical Applications of Copper Oxide Nanoparticles: An Expanding Horizon. ACS Biomaterials Science & Engineering 5, 1170-1188.

Vimala Devi, L., Sellaiyan, S., Selvalakshmi, T., Zhang, H.J., Uedono, A., Sivaji, K., Sankar, S., 2017. Synthesis, defect characterization and photocatalytic degradation efficiency of Tb doped CuO nanoparticles. Advanced Powder Technology 28, 3026-3038.

Wang, J., Zhang, S., Cao, H., Ma, J., Huang, L., Yu, S., Ma, X., Song, G., Qiu, M., Wang, X., 2022. Water purification and environmental remediation applications of carbonaceous nanofiber-based materials. Journal of Cleaner Production 331, 130023.

Wang, L., Si, W., Tong, Y., Hou, F., Pergolesi, D., Hou, J., Lippert, T., Dou, S.X., Liang, J., 2020a. Graphitic carbon nitride (g-C_3N_4)-based nanosized heteroarrays: Promising materials for photoelectrochemical water splitting. Carbon Energy 2, 223-250.

Wang, N., Zhang, F., Mei, Q., Wu, R., Wang, W., 2020b. Photocatalytic TiO_2/rGO/CuO Composite for Wastewater Treatment of Cr(VI) Under Visible Light. Water, Air, & Soil Pollution 231, 223.

Wang, Y., Lany, S., Ghanbaja, J., Fagot-Revurat, Y., Chen, Y., Soldera, F., Horwat, D., Mücklich, F., Pierson, J., 2016. Electronic structures of Cu_2O, Cu_4O_3, and CuO: A joint experimental and theoretical study. Physical Review B 94, 245418.

Wasewar, K.L., Singh, S., Kansal, S.K., 2020. Chapter 13 - Process intensification of treatment of inorganic water pollutants. in: Devi, P., Singh, P., Kansal, S.K. (Eds.). Inorganic Pollutants in Water. Elsevier, pp. 245-271.

Weldegebrieal, G.K., 2020a. Photocatalytic and antibacterial activityof CuO nanoparticles biosynthesized using Verbascum thapsus leaves extract. Optik 204, 164230.

Weldegebrieal, G.K., 2020b. Synthesis method, antibacterial and photocatalytic activity of ZnO nanoparticles for azo dyes in wastewater treatment: a review. Inorg Chem Commun 120, 108140.

Weldegebrieal, G.K., Dube, H.H., Sibhatu, A.K., 2021. Photocatalytic activity of CdO/ZnO nanocomposite for methylene blue dye and parameters optimisation using response surface methodology. International Journal of Environmental Analytical Chemistry, 1-23.

Weldegebrieal, G.K., Sibhatu, A.K., 2021. Photocatalytic activity of biosynthesized α-Fe_2O_3 nanoparticles for the degradation of methylene blue and methyl orange dyes. Optik 241, 167226.

Wenten, I.G., Khoiruddin, K., Wardani, A.K., Widiasa, I.N., 2020. Chapter 5 - Synthetic polymer-based membranes for heavy metal removal. in: Ismail, A.F., Salleh, W.N.W., Yusof, N. (Eds.). Synthetic Polymeric Membranes for Advanced Water Treatment, Gas Separation, and Energy Sustainability. Elsevier, pp. 71-101.

Xu, Q., Zhang, L., Cheng, B., Fan, J., Yu, J., 2020. S-Scheme Heterojunction Photocatalyst. Chem 6, 1543-1559.

Xu, Z., Xu, J., Ni, J., Hu, F., Xu, J., 2019. Visible Light Catalytic Reduction of Cr(VI) by Palygorskite Modified with CuO in the Presence of Tartaric Acid. Environmental Engineering Science 36, 491-498.

Xu, Z., Yu, Y., Fang, D., Liang, J., Zhou, L., 2016. Simulated solarlight catalytic reduction of Cr(VI) on microwave–ultrasonication synthesized flower-like CuO in the presence of tartaric acid. Materials Chemistry and Physics 171, 386-393.

Yang, Z., Yang, Y., Zhu, X., Chen, G., Zhang, W., 2014. An outward coating route to CuO/MnO_2 nanorod array films and their efficient catalytic oxidation of acid fuchsin dye. Industrial & Engineering Chemistry Research 53, 9608-9615.

Yao, L., Yang, H., Chen, Z., Qiu, M., Hu, B., Wang, X., 2021. Bismuth oxychloride-based materials for the removal of organic pollutants in wastewater. Chemosphere 273, 128576.

Yu, J., Zhuang, S., Xu, X., Zhu, W., Feng, B., Hu, J., 2015. Photogenerated electron reservoir in hetero-p–n CuO–ZnO nanocomposite device for visible-light-driven photocatalytic reduction of aqueous Cr(vi). Journal of Materials Chemistry A 3, 1199-1207.

Yu, S., Tang, H., Zhang, D., Wang, S., Qiu, M., Song, G., Fu, D., Hu, B., Wang, X., 2022. MXenes as emerging nanomaterials in water purification and environmental remediation. Science of The Total Environment 811, 152280.

Yugandhar, P., Vasavi, T., Shanmugam, B., Devi, P.U.M., Reddy, K.S., Savithramma, N., 2019. Biofabrication, characterization and evaluation of photocatalytic dye degradation efficiency of Syzygium alternifolium leaf extract mediated copper oxide nanoparticles. Materials Research Express 6, 065034.

Zhang, S., Wang, J., Zhang, Y., Ma, J., Huang, L., Yu, S., Chen, L., Song, G., Qiu, M., Wang, X., 2021. Applications of water-stable metal-organic frameworks in the removal of water pollutants: A review. Environmental Pollution 291, 118076.